Vat Photopolymerization 3D Printing of Advanced Soft Sensors and Actuators: From Architecture to Function

Wenyu Zhao, Ziya Wang, Jianpeng Zhang, Xiaopu Wang, Yingtian Xu, Ning Ding,* and Zhengchun Peng*

Fabrication and assembly of flexible sensors and soft actuators play important roles in improving the performance of wearable electronics and soft robots. Traditional manufacturing techniques have limitations in controlling the geometry and architecture of many soft actuation and sensing systems, which compromise their performance as well as applications. With the emergence of 3D printing, directly transforming 3D models into real objects becomes possible. In particular, vat photopolymerization techniques, represented by stereolithography, are capable of printing all-in-one and lab-on-a-chip devices with fast speed and high accuracy. Novel polymer formulations, including functional resins, hydrogels, elastomers, polymer blends, composites, and biological materials, have been developed for vat photopolymerization 3D printing to produce highly stable architectures, which prompts a remarkable revolution in mechanics and materials for soft electronics. This review looks into the recent developments of vat photopolymerization 3D printing technology for lightweight engineering, personalized electronics, and soft robots.

1. Introduction

Since Blytth and Hoffmann obtained a clear glass-like product from styrene in 1845, photopolymerization has been studied extensively and has become a practical technique for processing polymers.[1] Compared to other methods, it allows a unique spatial and temporal control of the process. Unlike heat-induced

or spontaneous chemical reactions, photopolymerization can be paused or resumed simply by switching the exposed light, and spatial control can be facilitated by using masks or focal light. During the development of photopolymerization, 2D manufacturing technologies that deposit polymers onto a substrate were realized first. Then, with further improvement of spatial and temporal controllability, various 3D (additive manufacturing (AM)) and even 4D (stimuli-responsive 3D printing) manufacturing technologies emerged. Specifically, according to the classification of International Organization for Standardization (ISO)/American Society for Testing and Materials (ASTM) 52900:2015 standard, the major AM process based on photopolymerization is called vat photopolymerization (VP), which selectively converts photocurable resins to solid polymers by polymerization under ultraviolet (UV, mostly ≤405 nm). This technology demonstrates high adaptability to print materials layer-by-layer with high-speed, high-resolution, high-accuracy, and good surface finish.[2] Furthermore, controlling the intensity or wavelength of light exposure in the single-component resin systems, and switching vats of resins during printing via complex equipment were adopted to further improve the temporal and spatial control of the manufacturing. Graded materials printing,[3] multi-wavelength VP printing,[4] and multimaterial printing were also developed,[5] which enable heterogeneity in all directions.

Whereby, VP has shown great potential in wearable electronics, microfluidics, robots, and many other fields. Among these applications, sensors and actuators are basic components to perceive the external environment and respond to external stimuli,[6] and they are usually the most integrated and functional devices in the system that can best reflect the advantages of materials and technological progress. As **Figure 1** shows, this review takes the theme of photopolymerization-based 3D printing technology and attempts to explore how it promotes the advancement of sensors and actuators. The flexibility of the material, for example, ensures desirable deformation, compliance, and comfort for pressure and strain sensors in different applications,[7] ranging from health and motion monitoring,[8] human skin mimicking,[9] to the expansion of the tactile sense of human,[10] and the tactile perception in prosthetics and robots.[11] As for actuators, the ability to

W. Zhao, Dr. Z. Wang, Dr. X. Wang, Y. Xu, Dr. N. Ding
Shenzhen Institute of Artificial Intelligence and Robotics for Society
Shenzhen 518129, P. R. China
E-mail: dingning@cuhk.edu.cn

Dr. J. Zhang, Prof. Z. Peng
Center for Stretchable Electronics and Nano Sensors
Key Laboratory of Optoelectronic Devices and Systems
of Ministry of Education
College of Physics and Optoelectronic Engineering
Shenzhen University
Shenzhen 518060, P. R. China
E-mail: zcpeng@szu.edu.cn

Dr. N. Ding
Institute of Robotics and Intelligent Manufacturing
The Chinese University of Hong Kong, Shenzhen
Shenzhen 518172, P. R. China

**ADVANCED
SCIENCE NEWS**

www.advancedsciencenews.com

**ADVANCED
MATERIALS
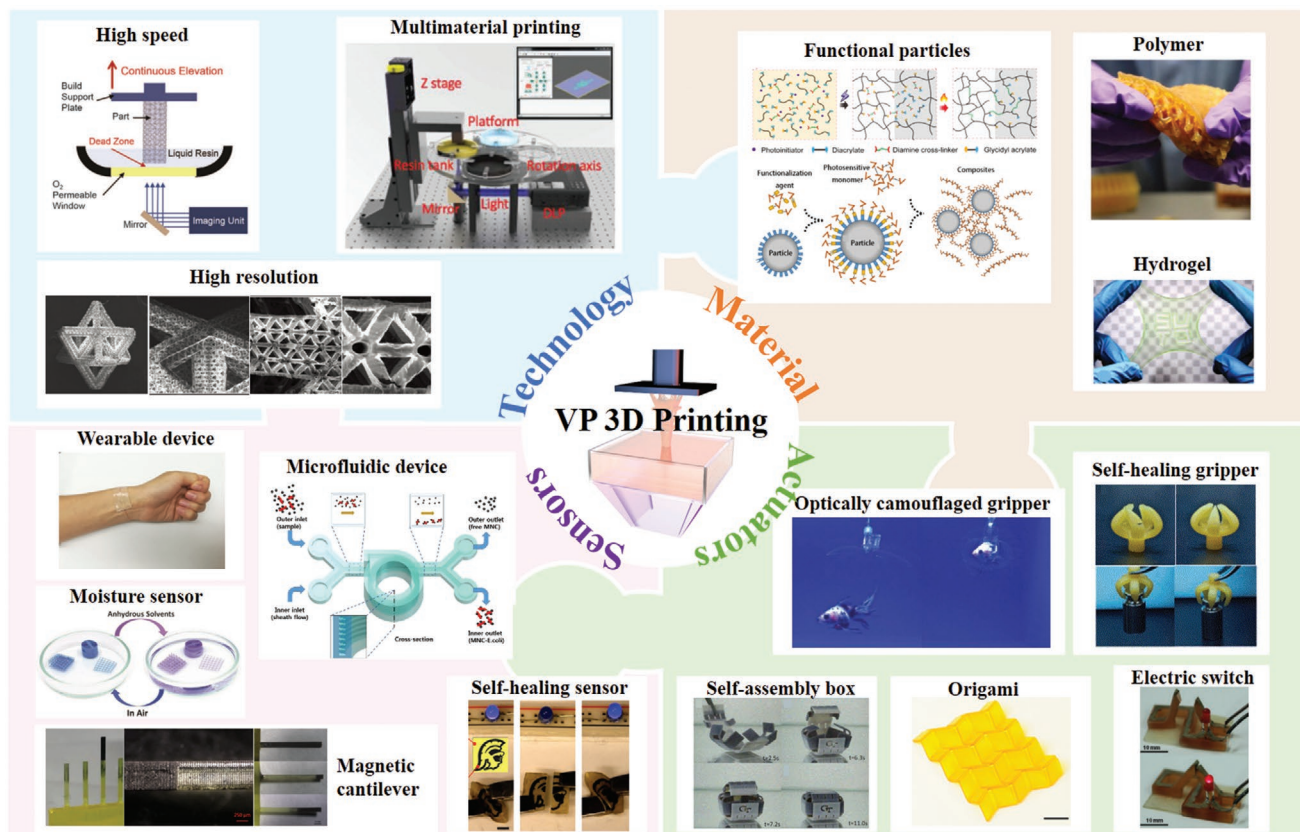TECHNOLOGIES**

www.advmattechnol.de

Figure 1. Schematic overview of VP 3D printing with their subcomponents: technology, materials, sensors, and actuators. High speed. Reproduced with permission.[23] Copyright 2015, AAAS. Multimaterial printing. Reproduced with permission.[11] Copyright 2019, Wiley-VCH. High resolution. Reproduced with permission.[244] Copyright 2016, Springer Nature. Functional particles. Reproduced with permission.[57a] Copyright 2019, Springer Nature. Polymer. Reproduced with permission.[245] Copyright 2019, AAAS. Hydrogel. Reproduced with permission.[246] Copyright 2018, Royal Society of Chemistry. Wearable device. Reproduced with permission.[54] Copyright 2019, Royal Society of Chemistry. Microfluidic device. Reproduced under the terms of the CC-BY Creative Commons Attribution 4.0 International License.[149] Copyright 2015, The Authors. Springer Nature. Moisture sensor. Reproduced with permission.[107] Copyright 2019, Wiley-VCH. Magnetic sensor. Reproduced with permission.[105] Copyright 2016, American Chemical Society. Self-healing sensor. Reproduced under the terms of the CC-BY Creative Commons Attribution 4.0 International License.[5] Copyright 2019, The Authors. Springer Nature. Optically camouflaged gripper. Reproduced under the terms of the CC-BY Creative Commons Attribution 4.0 International License.[234d] Copyright 2017, The Authors. Springer Nature. Self-healing gripper. Reproduced with permission.[184] Copyright 2019, American Chemical Society. Self-assembly box. Reproduced under the terms of the CC-BY Creative Commons Attribution 4.0 International License.[180] Copyright 2015, The Authors. Springer Nature. Origami. Reproduced with permission.[219] Copyright 2017, Wiley-VCH. Electric switch. Reproduced with permission.[15c] Copyright 2016, Wiley-VCH.

deform continuously and dexterously in confined space and on nonplanar surfaces is required to complete dynamic tasks.[12] For those used in human–machine interfaces, flexibility leads to better security for both actuators and humans.

However, as with all the other technologies, the processable materials for VP are limited, making flexible sensors and actuators manufacturing very difficult. The limitations mainly come from: 1) photopolymerization mechanism can only be free of radical polymerization or cationic polymerization. 2) The spectrum and intensity region of the printer's light source are fixed. 3) The photopolymer should be liquid with good fluidity to allow recoating of the build area.[13] Therefore, developing photopolymers with different compositions (monomers/oligomers, photoinitiator, absorber, functional fillers, etc.), and optimizing VP technology are significant. As summarized in Figure 1, various kinds of functions such as electrical conductivity, magnetic property, piezoelectricity,

self-healing, biocompatibility, moisture sensing, and 4D printing related stimulus-responsive effects are achieved by the intrinsic property of the monomer, the functional fillers, and the chemical bonding or special microstructure formed during photopolymerization. Especially when using conductive or magnetic particles as fillers, in addition to providing corresponding properties, they can also form directional arranged anisotropic structures by applying electric or magnetic fields.[14] VP also controls the degree of crosslinking and curing depth of the photocurable resins or composites with fillers through printing parameters (exposure light, time of exposure, temperature, etc.), to realize the functional structure with mechanical gradient.[15a] Thanks to the advanced spatial control of VP, porous flexible sensors, microfluidic device-based biosensors, self-assembly boxes, origami structures, switches, and grippers are achieved as shown in Figure 1.

Herein, we first introduce the representative VP technologies, their working principle, and characteristics in Section 2. Following that, in Section 3.1, the latest developments of VP-based pressure and strain sensors are categorized and introduced, respectively, according to their sensing mechanisms, including piezoresistive, capacitive, and piezoelectric. After that, the other sensing applications of VP are introduced, which include acoustic and magnetic sensors (Section 3.2), moisture and pH sensors (Section 3.3), and microfluidic device-based biosensors (Section 3.4). Then VP-based 4D printing and various stimuli-responsive actuators are reviewed, including temperature-induced actuation (Section 4.1), light-induced actuation (Section 4.2), moisture- or solvent-induced actuation (Section 4.3), electricity-induced actuation (Section 4.4), magnetism-induced actuation (Section 4.5), and pneumatic and hydraulic actuation (Section 4.6). Finally, we summarize the major material and technical challenges of VP and discuss the prospects and future research directions in soft sensor and actuator manufacturing.

2. Overview of 3D Printing Technologies via Photopolymerization

Stereolithography (SLA), as the primary AM technology, is the most well-known and wildly used VP-based 3D printing technology.[16] Typically, a standard SLA 3D printer consists of a laser light source, an optical controller, a movable platform, and a vat of resin.[17] When the printing process begins, the surface height of the resin is exactly one-layer thickness above the platform and the laser quickly scans and cures the first layer of the object along a controlled path. In the same way, objects are printed layer-by-layer until the overall shape is finished.[17] Through this formation mechanism and the high-resolution liquid–solid transition, VP technology enables accurate control of the processed soft material and avoids the deformation caused by the flow of the fluid material during the processing.

Based on SLA technology, another point-by-point printing technology named two-photon lithography (TPP) was developed with ultrahigh-resolution (200 nm).[18] Instead of curing and stacking resin in the z-direction, TPP technology uses ultrafast pulsed lasers to generate two very high flux of photons with longer wavelengths (780–820 nm), curing only occurs in a tiny region near the focal point of the lasers,[19] thus 3D microstructures could be fabricated effectively without the staircase effect or eliminate errors caused by fluctuations of the resin.[20]

Different from point-by-point printing, digital light processing (DLP) uses a digital projector instead of a laser as the light source to solidify one layer in every single exposure, which considerably shortens the printing process. Besides, a digital micromirror device or liquid crystal display can be used to control the projection light to selectively cure liquid photopolymer resin.[21] Within the DLP-based 3D printing technologies, projection microstereolithography (PμSL) achieved printing with higher resolution (up to 0.6 μm) by improvements in the correct exposure and layer thickness control.[22] Another developed DLP method named continuous liquid interface production (CLIP), which has a "dead zone" at the window of the vat, achieves printing with a smoother surface and unique high speed (1000 mm h^{-1} in the z-direction).[23] Feature resolution of CLIP in the z-direction is improved by projected light images that can change continuously.[24]

Photopolymer jetting (Polyjet), introduced by Objet Geometries in 2000, is a material jetting type of 3D printing technology for processing photocurable materials through photopolymerization. In this review, its application in sensor and actuator manufacturing will be mentioned as a necessary supplement to the VP technology because of its unique advantages.[25] During printing, the photosensitive polymer material is sprayed layer-by-layer onto the platform by a nozzle, and each layer is immediately solidified by UV light, resulting in a fully solidified model.[26] As a material jetting type of 3D printing technology, Polyjet could deal with photopolymers with higher viscosity, and the accuracy mainly affected by the size of its nozzle. More importantly, it is convenient for multimaterial printing by adding printhead, thus, it can be used to print more integrated sensors and actuators that have components made of different photopolymers.[27] **Figure 2** demonstrates all these photopolymerization-based 3D printing technologies.

The variety of VP and Polyjet technologies guarantee the diversity of flexible photocurable materials,[25] realize the rapid manufacture of sophisticated and complex structures, and provide the possibility for sensors and actuators with integrated architecture and outstanding performance in the future.

3. Fabrication of Sensors via VP

A sensor is an input device that utilizes sensitive materials based on physical or chemical effects to provide a processable output signal or information in response to a specific variable (such as pressure, temperature, magnetic field, and chemical or biotic components).[28] VP has been used to print structural components such as cantilever beams, microfluidic devices, molds for casting, or any other shape of platforms for sensors. However, a fully VP-printed sensor with a homogeneous structure usually requires functionalized photocurable materials and appropriate printing parameters.

Various resins were functionalized by adding fillers, and commercial resins were modified to be photocurable by selecting and combining appropriate photoinitiators and light absorbers.[29] Notably, hydrogels, crosslinked 3D networks of highly hydrophilic polymers, are processable for VP and widely used in sensing applications not only due to their intrinsic excellent flexibility, biocompatibility, and selective permeability,[30] but also due to the potential of multifunctionalization, including high transparency, conductivity, tunable mechanical properties, and self-healing ability.[31] Reasonable configuration allows full use of functional materials and structural materials in providing perception and flexibility. Therefore, the precise spatial control of VP to materials plays an important role in sensor manufacturing, especially for microfluidic device-based biosensors.

In this section, recent progress and applications of VP methods in manufacturing pressure and strain sensors will be introduced first. Other types of sensors, such as acoustic sensors, magnetic sensors, pH and moisture sensors, and microfluidic device-based biosensors and particle sensors will be separately discussed as well.
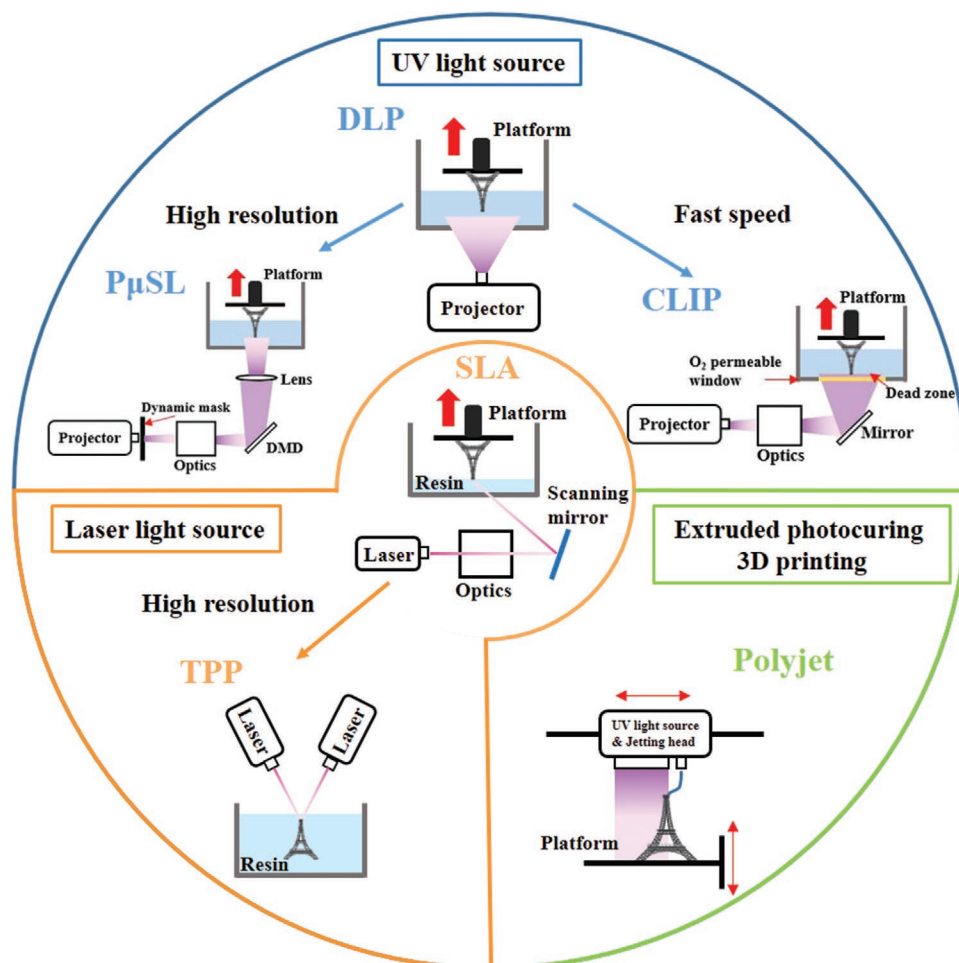
Figure 2. Schematic diagrams of five types of VP printers and a Polyjet printer.

3.1. Pressure and Strain Sensing

According to the structure and working principle, three types of pressure and strain sensors will be reviewed including: piezoresistive sensors, capacitive sensors, and piezoelectric sensors. Each type of sensor can be roughly classified as sensing components, structural components, and electrode components. Considering flexibility, polymer and hydrogel are commonly used as an elastic body or dielectric layer of the flexible sensors, which include polydimethylsiloxane (PDMS),[32] polyurethane (PU),[33] polyacrylamide (PAAm),[34] polyimide,[35] and Ecoflex.[36] While the conductive component could be obtained through fillers such as carbon nanotube (CNT),[37] graphene,[38] and Au/Ag nanowires and nanoparticles,[39] or directly obtained through conductive polymers, such as polyaniline,[40] polypyrrole,[41] and poly(3,4-ethylenedioxythiophene) polystyrene sulfonate (PEDOT:PSS).[42]

However, not all of the polymers or fillers mentioned are processable for VP, more importantly, the sensing material is often the key to determine the sensor performance. Therefore, methods such as hybrid printing,[43] post-treatments, multimaterial printing,[44] and composite resin development[45] have been studied as solutions to realize the conductivity and

sensitivity of the photocurable materials recently.[46] Different types of sensors with different materials, performance, and applications are summarized and presented in **Table 1**. The application of VP in the manufacturing of pressure and strain sensors are reviewed according to the sensing mechanisms.

3.1.1. Piezoresistive Sensors

As **Figure 3**a shows, piezoresistive sensors transduce external forces into resistance changes of the sensing material.[60] In general, the resistance change of piezoresistive sensors can be derived from the contact resistance between the sensing material and the electrode or the volume resistance within the sensing material.[9] Contact resistance changes tend to larger changes than volume resistance changes at the same pressure. Therefore, a high sensitivity piezoresistive sensor usually contains a sensing layer with a rough surface (for example, an array of microdomes, micropyramids, or micropillars), furthermore, the hollow structure can be adopted for more compressibility and sensitivity as well, all of which are easy to achieve in 3D with VP. Besides, VP's ability to prototype in a fast and relatively inexpensive way can speed sensor structure optimization and iteration.

Table 1. Summary of the recent reported pressure and strain sensors fabricated by photopolymerization-based 3D printing.

Material	Method	Performance	Application	Refs.
PUA[a]/PEDOT:PSS	DLP	Sensitivity: 1.666×10^{-4} S N^{-1} m^{-1}	Piezoresistive pressure sensor	[47]
PPTMGA[b]-40/ionic hydrogel (PEGDA[c]/LiCl)	DLP	Tensile strength: 15.7 MPa Elongation: 400% Pressure sensitivity: 2010.1 MPa^{-1}	Piezoresistive stretchable stain sensor, electric switch, wearable device	[48]
MPS[d]/VPS[e]/CNT	DLP	Elongation: 1400%	Electric switch	[49]
EAA[f]/AUD[g]/Ag	DLP	Elongation: 1100%	Electric switch and pneumatically actuated soft actuator	[50]
HDDA[h]/PDMS/carbon grease	DLP	Tensile strength: 17.4 kPa	Self-healable actuator, stretchable piezoresistive strain sensor	[51]
MJ resin/GNs[i]	DLP	Density: 1.06 g cm^{-3} Fracture toughness: 1.59 MPa $m^{1/2}$	Anisotropic electrical conductor, self-sensing smart helmet	[52]
Resin(Are3d-dlp405)/MWCNTs[j]	DLP	Elongation: 100%	Capacitive pressure sensor	[53]
PAAm–PEGDA/$MgCl_2$/VHB tape	DLP	Sensitivity: 0.84 kPa^{-1}	Capacitive pressure/strain sensor, wearable devices	[54]
PAAm–PEGDA/$MgCl_2$/WPUA[k]	DLP	Sensitivity: 0.61 kPa^{-1} Signal drift: <5%	Capacitive pressure/strain sensor, wearable devices	[55]
PEGDA/$BaTiO_3$	DPP	Piezoelectric coefficients: ≈40 pC N^{-1}	Piezoelectric devices	[56]
TMSPM[l]/PZT[m]	PµSL	Lattice overall dimension, modulus, and piezoelectric charge constant: ≈42 pC N^{-1}	Piezoelectric location and directionality sensing, self-sensing boxing glove, air pressure detector	[57]
TMSPM/BNNT	PµSL	Sensitivity: 24 mV kPa^{-1}	Piezoelectric pressure sensor	[58]
HDDA/PVDF[n]	PµSL	Piezoelectric voltage coefficient: 105.12×10^{-3} Vm N^{-1}	Piezoelectric pressure sensor	[59]

[a]Polyurethane acrylate; [b]Poly(tetrahydrofuran); [c]Poly(ethylene glycol) diacrylate; [d]Mercaptan-functionalized polysiloxane; [e]Vinyl-terminated poly-(dimethylsiloxane); [f]Epoxy aliphatic acrylate; [g]Aliphatic urethane diacrylate; [h]1,6-hexanediol diacrylate; [i]Graphene nanoplatelets; [j]Multiwall carbon nanotubes; [k]Water-dilutable polyurethane acrylate; [l]3-(trimethoxysilyl)propyl methacrylate; [m]Lead zirconate titanate; [n]Polyvinylidene fluoride.

Considering the complexity of the system, it is difficult to implement highly integrated functional devices with fully VP printing, therefore, coordination with other technologies, such as Polyjet, fused deposition modeling, and inkjet, becomes a convenient option.[61] To improve the stability of the interface between the structural part and the sensing part, Zhou et al. proposed a sensor composed of SLA-printed membrane with patterned microchannel and filled Galinstan as the sensing material.[62] Depending on the asymmetric arrangement of the surface wiring, the sensor exhibits different responses toward bending with different angles and directions. Hagihghi et al. proposed a flow sensor consisting of an SLA 3D-printed hair cell and a piezoresistive micro-electromechanical systems-based liquid crystal polymer membrane.[63] The bending of the pillar hair cell causes a resistance change of attached strain gauges to quantitatively describe the rate of the flow. By assembling with tubes and capsules, the flow sensor can be used for real-time monitoring of intravenous infusion.

Function materials can be introduced by the post-treatment process as well.[64] Shao et al. fabricated a force sensor consisting of two parallel layers by a DLP 3D printer with polyurethane acrylate (PUA).[47] Micropyramid arrays were designed on the bottom layer to increase the variation of the contact area under the external force, and each layer was spin-coated with PEDOT:PSS film to be conductive.[47] Dip coating is another post-treatment method commonly used for fabricating conductive films. Peng et al. successfully synthesized three kinds of photocurable resins with great stretchability and elongation

(15.7 MPa and 414.3%, respectively) for DLP.[48] To fabricate a stretchable sensor, a photocurable ionic hydrogel (monomer acrylamide/LiCl) film was dip-coated with the printed elastomer PPTMGA as a conductor and maintain good transparency, as shown in Figure 3b.[48] Similarly, Zhao et al. developed a series of silicone elastomers with tunable mechanical properties, and a 3D-printed cellular was coated with a layer of CNT-doped hydrogel by dip coating to form a stretchable electric switch, as shown in Figure 3c, which can adjust the intensity of the LED by pressure applied.[49] In addition to ionic hydrogels and carbon-based conductors, metals and their compounds are the most well-known and commonly used fillers as well. For example, Patel et al. developed a novel highly stretchable and UV curable elastomer resin system consisting of a mixture of a monofunctional monomer consisting of epoxy aliphatic acrylate (EAA) and a difunctional crosslinker consisting of aliphatic urethane diacrylate (AUD).[50] By using a commercial DLP printer, a bucky-ball was printed and then immersed into a silver nanoparticles dispersion to make it conductive and used as an electric switch, as shown in Figure 3d. Electroless plating has proved as a universal, robust, and cost-effective approach for the fabrication of metallic coatings and it has been used in processing VP printing objects recently. For example, Wang et al. proposed a resin formulation containing Br-containing vinyl-terminated initiator that can occur surface-initiated atomic-transfer radical polymerization (ATRP).[65] Figure 3e shows the process of ATRP and the electroless plating that coated copper and nickel onto the printed complex structures, including
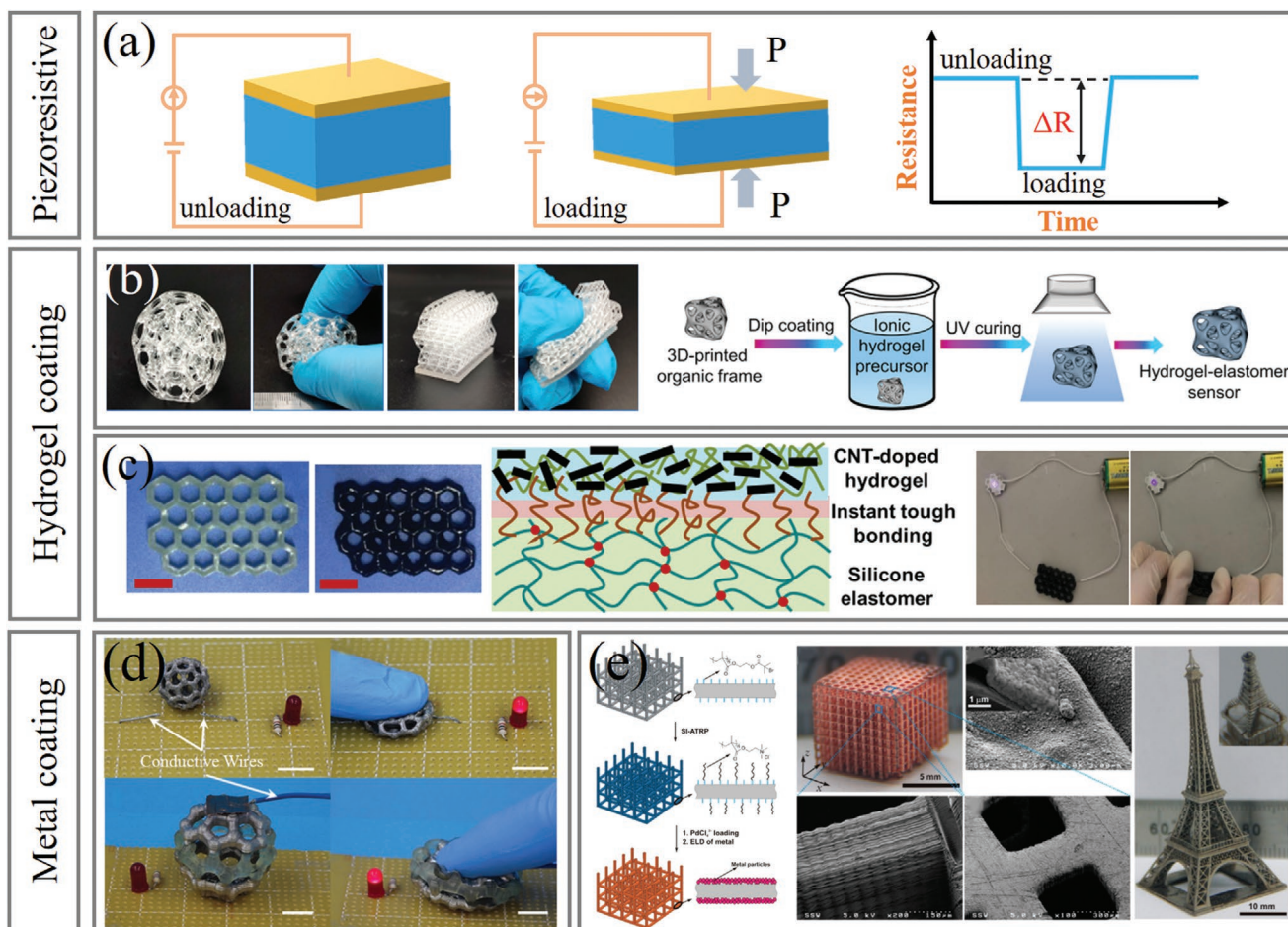
Figure 3. Post-treatment methods for integrating conductive additives. a) Sensing mechanism for the piezoresistive sensor. b) 3D-printed hollow structures made by PU elastomers with robustness and flexibility (left), and the process of dip coating the ionic hydrogel on the 3D-printed organic frame (right). Reproduced with permission.[48] Copyright 2020, American Chemical Society. c) Printed silicone elastomer coated with CNT-doped hydrogel layer (left), and a stretchable electric switch (right). Reproduced with permission.[49] Copyright 2019, American Chemical Society. d) A flexible Bucky-ball coated with silver nanoparticles as an electric switch. Reproduced with permission.[50] Copyright 2017, Wiley-VCH. e) The fabrication process of ATRP and electroless plating (left), a Cu-coated microlattice, and a Ni-coated Eiffel tower (right). Reproduced with permission.[65] Copyright 2014, American Chemical Society.

microlattices and even an Eiffel tower. Fantino et al. developed a more direct method that adding AgNO$_3$ to a PEGDA-based photocurable oligomer to generate silver nanoparticles in situ on the crosslinked polymer matrix by UV-irradiation (365 nm) after printing.[46] Although the UV degradation and the uncertainty of light penetration impact the performance, the idea of adding fillers into photocurable resins is desirable. However, peeling, breakage, or short circuit caused by residual trace metal particles seriously limit the application of such printed conductive objects. As a result, the insufficient stability and durability of such post-treatment processes may not meet the requirements of large and continuous deformation of the flexible sensors.[66]

Intrinsic conductivity can be obtained by adding conductive fillers to resins, however, it may induce a scattering effect that causes turbidity and limits the penetration depth and cure depth of the resin. Especially when adding metal particles, their high reflectivity in UV–vis range deprives the incident energy of the photosensitive resin, making the processing more

difficult.[67] Moreover, the increased viscosity caused by filler addition prevents recoating and reduces the molecular mobility in the printing process, slowing down the diffusion of active centers and decreasing the polymerization rate.[64] In most cases, developing functionalized printable resins often need the strictly selected composites and repeatedly tested proportions of each material.[64,68]

In addition to conductivity, the unique characteristics of natural biological tissue have inspired the development of new functional sensors.[69] Among them, self-healing is a valuable capability for the materials to improve the durability of the sensor. Self-healing of polymers can be achieved by a few categories of reactions, including covalent bonding, supramolecular chemistry, H-bonding, ionic interactions, and π–π stacking.[70] Yu et al. reported a method for manufacturing elastomer structures with self-healing ability, which relies on a molecularly designed elastomer ink with both thiol and disulfide groups to obtain photopolymerization and self-healing capacities, respectively.[51] After being doped with carbon-black, the elastomer
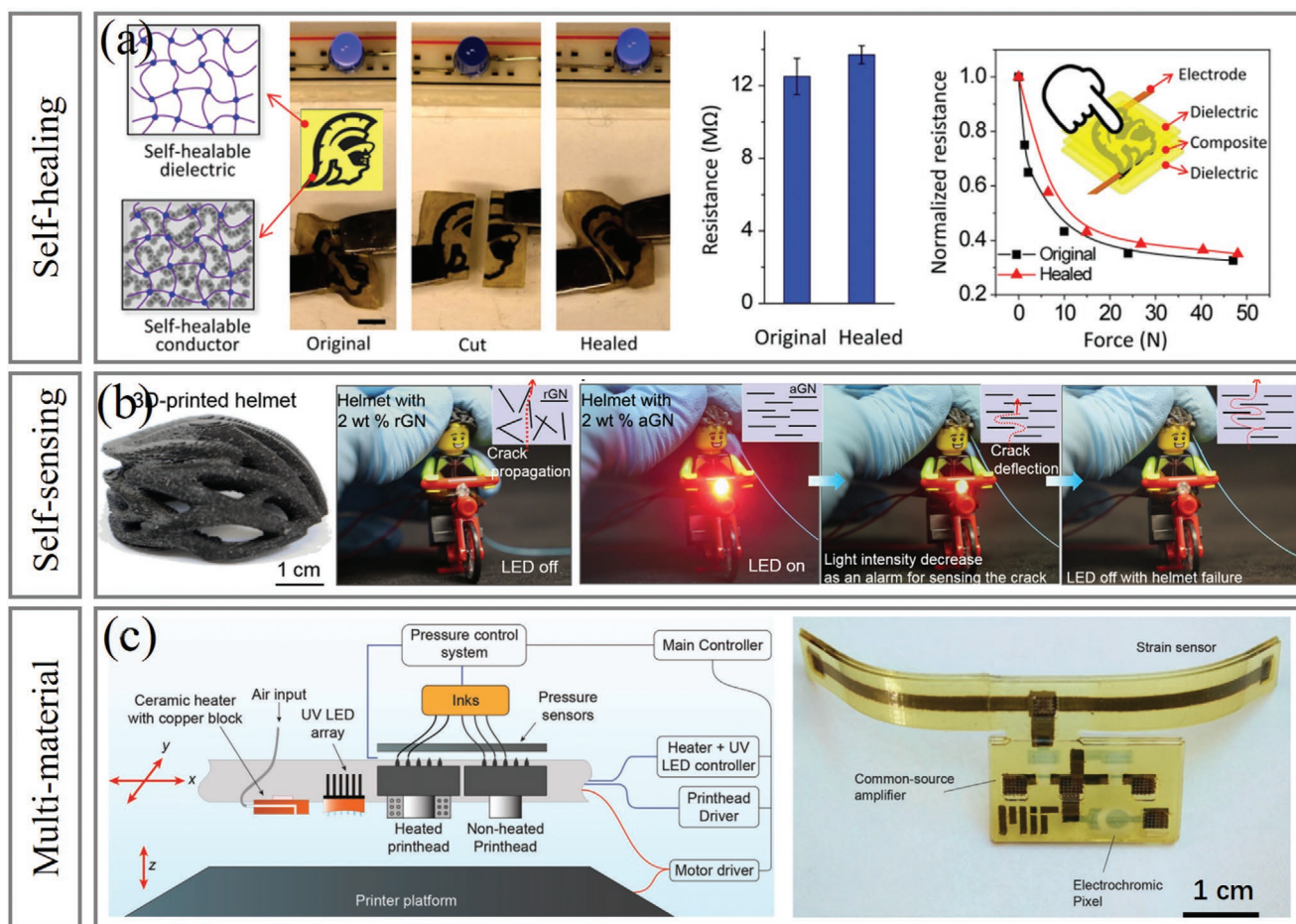
**ADVANCED
SCIENCE NEWS**

www.advancedsciencenews.com

**ADVANCED
MATERIALS
TECHNOLOGIES**

www.advmattechnol.de

Figure 4. Photopolymerization-based intrinsic conductive materials for multifunctional pressure sensors. a) The schematic illustration of the structure of self-healing elastomers and a flexible, self-healable conductor powered an LED (left), the resistance changes before and after self-healing, and the performance of a self-healed force sensor (right). Reproduced under the terms of the CC-BY Creative Commons Attribution 4.0 International License.[51] Copyright 2019, The Authors. Springer Nature. b) The 3D-printed self-sensing helmet and the demonstration of its different self-sensing properties with random GNs and aligned GNs. Reproduced under the terms of the Creative Commons Attribution NonCommercial License 4.0 CC BY-NC.[52] Copyright 2019, The Authors, AAAS. c) The schematic illustration of the printing platform (left), and the photograph of the fully 3D-printed autonomous sensory composite shows a strain sensor linked to an electrical amplifier (right). Reproduced with permission.[27a] Copyright 2017, Wiley-VCH.

resin was used to fabricate a force sensor that can remain good performance after self-healing, as shown in **Figure 4**a. This material system was proved capable of being printed into any complex shapes, which shows its potential for wider sensing applications.

Inspired by the hierarchical structure of nacre, Yang et al. developed an electrically assisted 3D printing method to fabricated a self-sensing helmet by photocurable resin containing aligned Graphene nanoplatelets (GNs).[52] As shown in Figure 4b, the aligned GNs generate the anisotropic electrical property of the structure and its resistance will increase as the crack formation, therefore, the brightness of LED connected to the helmet can reflect its damage. Besides, Polyjet-based 3D printing can realize multimaterial manufacturing simply by switching the printing head, making it easier to integrate functional components into a single device. Sundaram et al. developed a drop-on-demand multimaterial AM platform, as shown in Figure 4c, where each printhead can accept up to 10 different inks that can be extruded or dropped and simultaneously cured

under a UV LED array.[27a] With this printing platform, a multilayered device that containing strain-sensitive elements with an organic electrochemical transistor-based amplifier and an electrochromic element was fully printed without assembly or any other subsequent processing.

3.1.2. Capacitive Sensors

Generally, capacitive sensors transduce pressure or stretch input to a change in the capacitance of a parallel plate capacitor.[71] When tensile or compressive stress is applied to the structure of the capacitor, the elastic dielectric layer will be stretched or compressed accordingly, resulting in changes in electrode spacing and equivalent electrode area, which in turn leads to changes in the capacitance of the device and realizes the stress detection (**Figure 5**a). From a performance perspective, capacitive sensors exhibit high sensitivity and rapid response time,[72] and they are close to skin-type sensing behavior in terms of strain sensitivity,
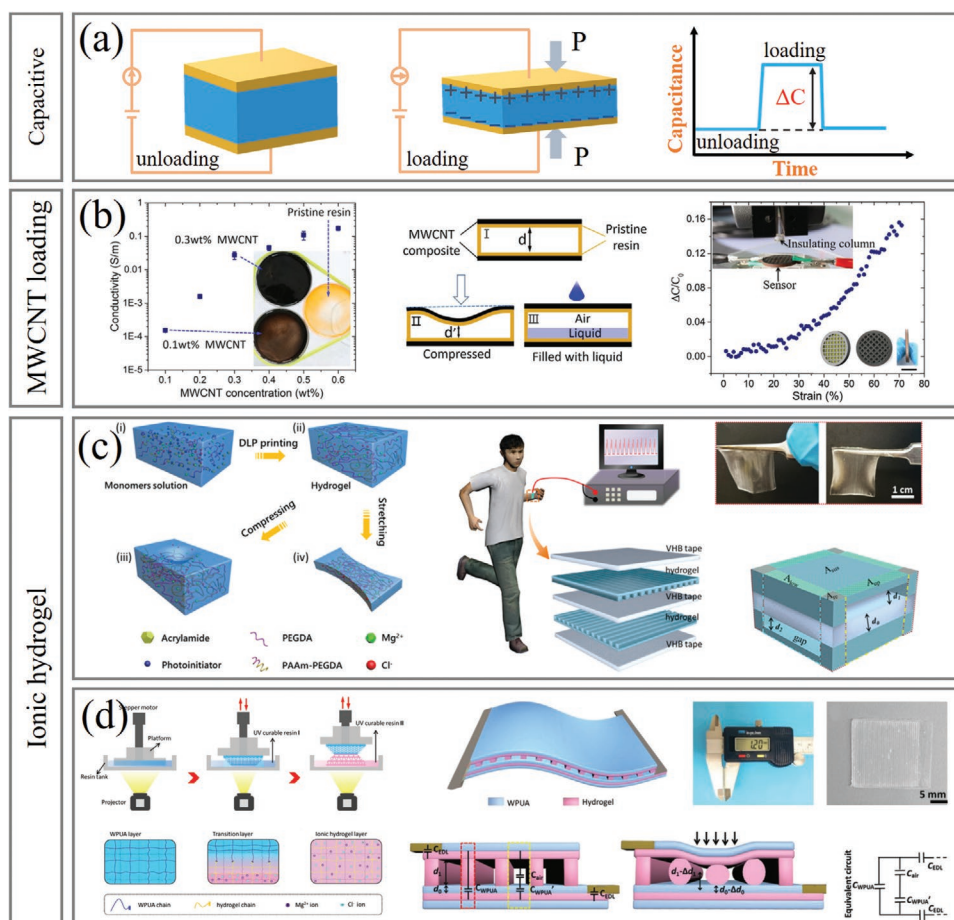
**ADVANCED
SCIENCE NEWS**

www.advancedsciencenews.com

**ADVANCED
MATERIALS
TECHNOLOGIES**

www.advmattechnol.de

Figure 5. VP-based capacitive sensors. a) Sensing mechanism for the capacitive sensor. b) Conductivity as a function of MWCNT loading, and images of pure resin and resin containing different amounts of MWCNT nanocomposites (left), and schematic of working principle of the hollow capacitive sensor and the sensing ability test (right). Reproduced with permission.[53] Copyright 2017, Elsevier. c) Schematic polymerization mechanism of a PAAm–PEGDA hydrogel network (left), and the design of the sensor and the optical images of structured hydrogel layer (right). Reproduced with permission.[54] Copyright 2019, Royal Society of Chemistry. d) Schematic illustration of the dual-material printing process and the all-printed capacitive sensor. Reproduced with permission.[55] Copyright 2019, Wiley-VCH.

pressure, and proximity sensing,[73] with low power consumption and independent operating temperature.[74]

Typically, the configuration of the capacitive sensor is that the dielectric medium is sandwiched between two electrode layers. This traditional hierarchical structure inevitably requires multimaterial printing. Accordingly, Mu et al. adopted the multi-vat approach, as Figure 5b shows, replacing the vat with a secondary material during the pause of printing to achieve fully printed capacitive strain sensors.[53] The pristine photocurable resin (Are3d-dlp405) was used as the dielectric layer and the resin incorporated with multiwalled CNTs (MWCNTs) was used as the electrodes. The hollow structure of the sensor can detect changes in the spacing between the two plates or changes in the level of liquid in between. The ability of the hollow capacitive sensor to detect force was tested and the capacitance dependence on strain was found to be up to 70% of nominal strain (Figure 5b). The performance can be further improved by manipulating the geometry to improve the compressibility of the dielectric layer.[75] When the dielectric layer is a bulk material, because the pressure applied is converted into internal

stress, designing voids into the dielectric layer through VP can achieve easier deformation and compression.

Hydrogels are promising candidate materials for VP methods to manufacture capacitive wearable sensors.[76] Despite that, the common hydrogel processing technologies, such as screen printing,[77] spin coating,[78] and photolithography,[79] have their own advantages in producing lamination structure for capacitive sensors, VP performs better in overcoming the lack of stiffness, manufacturing 3D characteristics and complex internal structures. In contrast, the resolution of the grid structure fabricated by extrusion-based 3D printers is low (usually greater than 100 μm), as a result, the ability in increasing sensitivity is limited and the printed devices are not comparable with the state-of-the-art capacitive sensors.[80] Figure 5c depicts a work done by Yin et al., who introduced two kinds of photosensitive hydrogels with different mechanical properties and copolymerized them to produce ionic conductive hydrogels (PAAm–PEGDA/MgCl$_2$) as transparent and flexible electrodes with microstructure, VHB tape was used as the dielectric layer and adhesive to

ADVANCED
SCIENCE NEWS
www.advancedsciencenews.com

ADVANCED
MATERIALS
TECHNOLOGIES
www.advmattechnol.de

constitute wearable capacitive sensor.[54] Cavities were formed by the hydrogel layer with microstructure, which decreases the initial capacitance of the devices but improves the sensitivity of the sensor. Identical sensing units were defined to simplify the construction of a theoretical prediction of capacitance for the sensor.

The physical bonding, together with the inconsistency of elasticity between the electrodes and the dielectric material, results in a relative dislocation between layers during repeated deformations, which usually generates remarkable signal drift and reduces the stability and reliability of the sensor.[81] Improving the adhesion between layers using stable chemical bonding is undoubtedly a good solution.[55] Yin et al. developed a PAAm/PEGDA/Mg^{2+} ionic hydrogel as the electrode, and a hydrogel compounded with WPUA was used as the dielectric component and seals to retard hydrogel dehydration.[55] As Figure 5d shows, the presence of acrylic groups in these two precursors, and their similar solvent polarity allow the different polymer layer to be cured directly onto the previous one via chemical bonding at the interface, which guarantees the stability and reliability of the structure under bending, compressing, twisting, and stretching. The composite remains attached even after dehydration of hydrogel as well. An all-printed five-layer structured capacitive sensor consisting of WPUA and ionic hydrogel with multiple parallel beams was printed (Figure 5d). Compared with the existing sensors involving electronic conductors, the VP-printed elastic hydrogel-based sensors have the advantages of ultrathin, transparency, and high tensile properties. Even more, they do not require tedious fabrication processes and get rid of the limitation of the significant increase in resistance during deformation.[30]

3.1.3. Piezoelectric Sensors

Piezoelectric materials can convert mechanical force into electricity and vice versa.[82] As **Figure 6**a shows, piezoelectric sensors are mostly used for dynamic sensing because of the impulsive signal generated by the piezoelectric material,[60] while they show a more precise response to external force and piezoelectric materials can generate voltage signals themselves without external energy sources.[83]

For piezoelectric materials, both organic (mostly polymers) and inorganic materials have been found to exhibit piezoelectricity and studied for pressure sensing, such as AlN,[84] ZnO,[85] PbTiO$_3$,[86] BaTiO$_3$,[87] PZT,[88] PVDF,[89] and poly(vinylidenefluoride-co-trifluoroethylene) (P(VDF-TrFE)).[90] In inorganic piezoelectric crystals, the arrangement of ions in noninversely symmetric structures of dielectric materials produces piezoelectric effects.[91] Most of the traditional piezoelectric materials are brittle ceramic materials, which have been reported to be printed in VP methods already.[92] BaTiO$_3$ is one of the most reported fillers used in piezoelectric formulations owing to its large piezoelectric, good electromechanical coupling coefficients and high dielectric permittivity.[93] Kim et al. demonstrated piezoelectric polymers composed of BaTiO$_3$ nanoparticles and photocurable polymer, such as PEGDA, and generated user-defined 3D microstructures by exposing them

to digital optical masks.[56] The main issue is the sediment and agglomeration of the piezoelectric particles directly mixed with photosensitive resins, resulting in a poor piezoelectric response. Solvents such as N, N-dimethylformamide,[94] diethyl fumarate, and BYK (a type of copolymer containing phosphoric acid groups) were used to disperse the piezoelectric material more uniformly and reduce the viscosity of the resin.[59,95] Wang et al. demonstrated an SLA-printed high-performance piezoelectric nanoceramic and investigated the effects of dispersant and rheological behavior of the BaTiO$_3$ suspensions.[96] The ceramics exhibit a piezoelectric constant of 163 pC N^{-1} and relative permittivity of 2762, respectively.[96]

PZT is another commonly used piezoelectric material, which is special for its large piezoelectric and electromechanical coupling coefficients. PZT-based sensors exhibit high sensitivity and stability, fast response, and low hysteresis.[97] Although it is rigid, PZT can be integrated into an ultrathin sheet of flexible equipment or other porous structured forms. Recently, Cui et al. have done remarkable work of showing a strategy to break through the limitations of the charge motion in traditional piezoelectric materials, which are dictated by their intrinsic crystals.[57a] A series of piezoelectric metamaterials were designed and shown in Figure 6b for tailorable piezoelectric charge constants that allow the user to specify piezoelectric responses to be amplified, reversed, or suppressed in the specified direction. Highly sensitive piezoelectric inks containing high concentrations of PZT nanoparticles were developed, and devices used for force amplitude and directional sensing, shock absorption, and self-monitoring, and position mapping were obtained by stacking different types of piezoelectric metamaterial units via a PµSL 3D printer. In another related work of them, Yao et al. used the same material and the printing system shown in Figure 6c to fabricate wearable piezoelectric devices with improved compliance.[57b] It is significant to combine high sensitivity and high compliance at the same time, because structural compliance and electromechanical coupling sensitivity are usually tightly coupled, and a high piezoelectric response comes at the cost of low flexibility. The functionalized PZT particles were mixed with UV-sensitive monomer matrix and printed as highly sensitive wearables that detect low pressure air (<50 Pa) coming from different directions, as well as wireless, self-sensing sporting gloves for simultaneous impact absorption and punching force mapping, as shown in Figure 6c.[57b]

Besides, Zhang et al. used boron nitride nanotubes, which have excellent mechanical properties, high thermal and chemical stabilities, good biocompatibility, and strong piezoelectricity, as the piezoelectric filler to overcome the limitation of traditional inorganic piezoelectric ceramics in conformal wearable electronic applications.[58] Figure 6d depicts a self-powered and conformal tactile sensor array printed by projection SLA to enable haptic sensing of robot hands and detect the spatial distribution of force on uneven surfaces.

Compared with inorganic piezoelectric materials, organic piezoelectric polymers are more promising for wearable pressure sensors due to their inherent flexibility. In organic piezoelectric polymers, the piezoelectric effect is caused by the molecular structure of the polymer and its orientation.[98] Among organic piezoelectric polymers, PVDF and
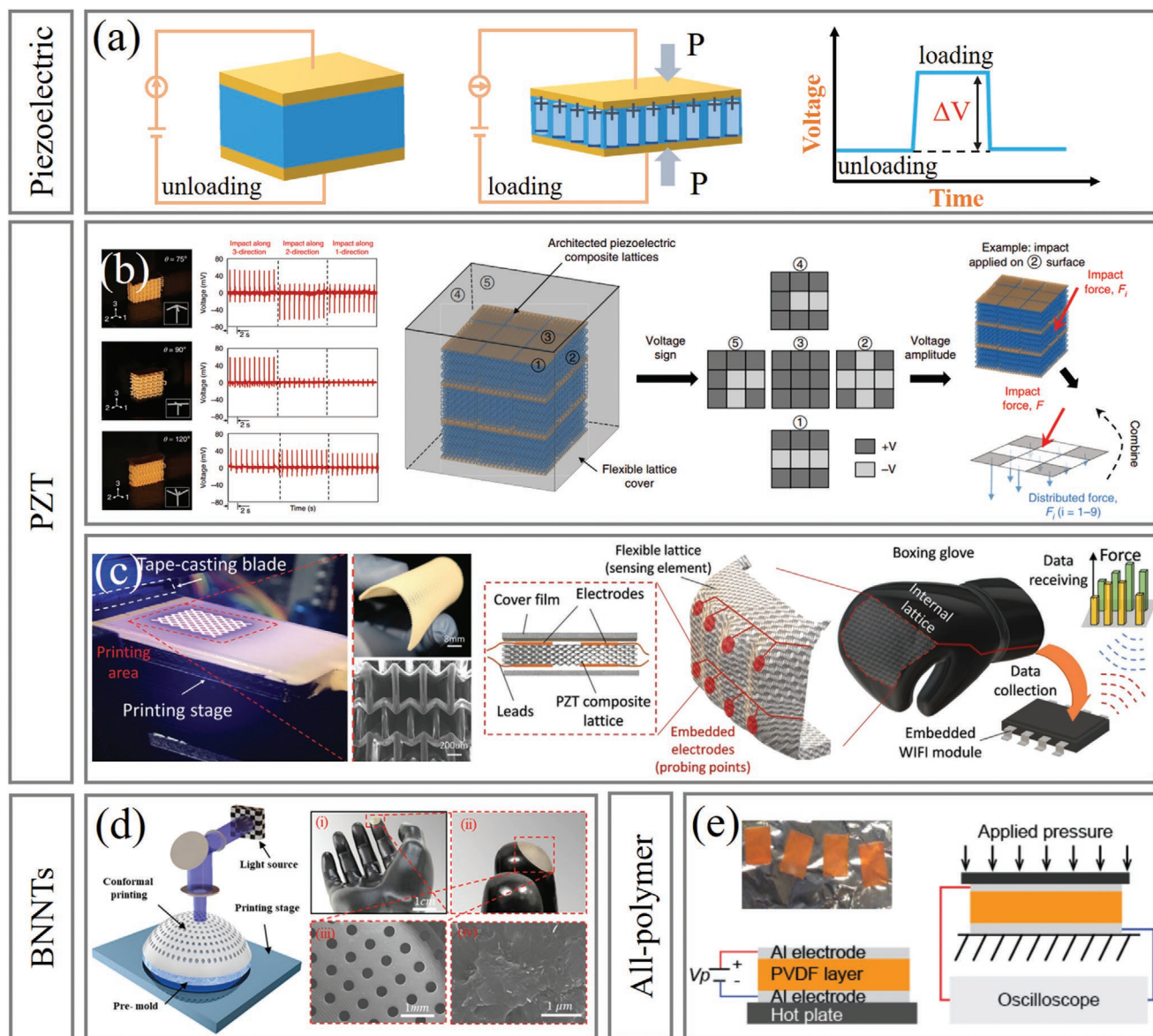
Figure 6. VP-based piezoelectric sensors. a) Sensing mechanism for the piezoelectric sensor. b) Piezoelectric metamaterials with the ability to identify forces with a certain direction (left), and a sensor using piezoelectric metamaterials stacked from four types of designed building blocks to sense arbitrary force directions (right). Reproduced with permission.[57a] Copyright 2019, Springer Nature. c) Custom PμSL fabrication system for piezoelectric nanocomposite with fine surface finish (left), and schematics of the wireless self-sensing boxing glove (right). Reproduced with permission.[57b] Copyright 2019, Wiley-VCH. d) Schematic illustration of the projection SLA system and the self-powered and conformal tactile sensor array. Reproduced with permission.[58] Copyright 2020, Elsevier. e) 3D-printed PVDF layer and the piezoelectric sensor. Reproduced with permission.[59] Copyright 2017, Elsevier.

its copolymers, such as P(VDF-TrFE), show great application potential due to their flexibility, durability, lightweight, photocurable, and chemical inertness.[99] Chen et al. developed a PVDF-based piezoelectric resin to manufacture flexible piezoelectric devices with customized geometries by using PμSL 3D printing.[59] As Figure 6e shows, 3D-printed PVDF thick films were utilized for piezoelectric sensors, and conductive aluminum layers were then attached to each side of the sample as electrodes. By increasing the concentration of PVDF and poling electric field, 3D-printed piezoelectric layer with maximum piezoelectric voltage coefficient of 105.12×10^{-3} Vm N^{-1} was demonstrated experimentally.[59]

In conclusion, the development of the photocurable functional material system is the key for fully VP-printed flexible pressure and strain sensors. This process is accompanied by tests of surface functionalization of fillers, chemical crosslinking between monomer matrix and functionalized fillers, complex component dosage testing and analysis, and control of resin viscosity. Appropriate structural design and convenient topology optimization achieved by VP can further improve the performance of sensing components and overall improve compliance and conformality of sensors. The progress of multimaterial printing technologies also lights up the future of VP to manufacture multifunctional, highly integrated pressure and strain sensors.
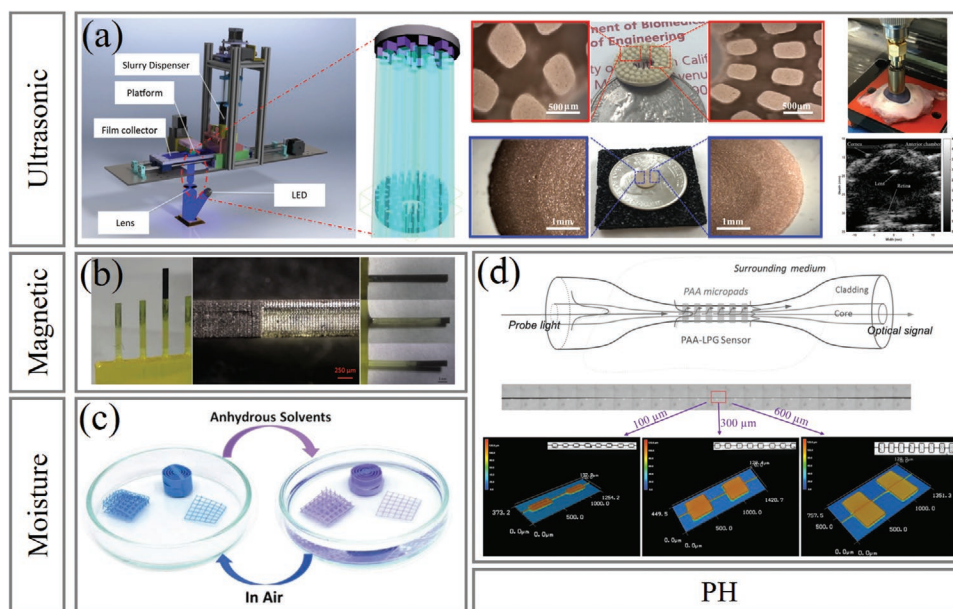
ADVANCED
SCIENCE NEWS
www.advancedsciencenews.com

ADVANCED
MATERIALS
TECHNOLOGIES
www.advmattechnol.de

Figure 7. VP-based acoustic, magnetic, and chemical sensing. a) Schematic illustration of the MIP-SL system (left), the printed segment annular array and a printed focused concaved-shape piezoelectric element, and a printing focused transducer for ultrasonic scanning of the porcine eye ball (right). Reproduced under the terms of the CC-BY Creative Commons Attribution 4.0 International License.[101] Copyright 2019, The Authors. Elsevier. b) Array of cantilevers with high-resolution features and varied lengths. Reproduced with permission.[105] Copyright 2016, American Chemical Society. c) Different architectures of the 3D-printed CP1 in the air at 25 °C (blue color), and introduced in dry solvents such as ethanol, methanol, tetrahydrofuran, or acetonitrile (violet color). Reproduced with permission.[107] Copyright 2019, Wiley-VCH. d) The microfiber pH sensor based on micropatterned PAA ionic hydrogel. Reproduced with permission.[110] Copyright 2016, Wiley-VCH.

3.2. Acoustic and Magnetic Sensing

The conversion of electricity and mechanical force by piezoelectric effect is bidirectional, in contrast to piezoelectric sensors, the conversion from electricity to mechanical force can be used as piezoelectric microphones and used in ultrasonic nondestructive sensing.[100] Chen et al. demonstrated an annular piezoelectric array and a printing focused concaved-shape piezoelectric element consisting of $BaTiO_3$ nanoparticles printed by mask-image-projection-based SLA (MIP-SL), as shown in **Figure 7**a.[101] The printed elements were assembled into the ultrasonic array transducer to improve the lateral resolution and depth of field, and a porcine eyeball was ultrasonic scanned by a printed focused transducer, which provides an option to realize the function assembly of 3D geometry structure conveniently and effectively.

The oxides of iron and other metals are a common class of magnetic materials, of which Fe_3O_4 is the best known.[102] Both the size and concentration of the magnetic fillers affect the uniform dispersion and avoidance of agglomeration, therefore, Fe_3O_4 nanoparticles are used to improve the processability.

Recently, studies were made on the application of magnetic particles include printing reinforced materials by controlling the orientation of the magnetic particles,[103] printing materials with tunable mechanical and magnetic properties and printing multilayered magnetic soft actuators.[104] While for sensing application, a simple method is to measure the magnitude of the magnetic field by observing the deflection of the cantilever beam made by magnetic sensitive materials. To achieve this goal, Credi et al. developed a UV-curable system by blending a bifunctional acrylic monomer with a photoinitiator and visible dye to ensure the structure of the microcantilever array, as shown in Figure 7b.[105] Two strategies, the electroless plating process to deposit a thin layer of metal alloy on the microcantilever, and loading magnetite nanoparticles (magnetic iron (II, III) oxide nanopowder) within the polymer matrix, were implemented, respectively. By using the magnetic field to drive the cantilever beams, the sensing property of static bending behavior is qualitatively studied and the results show that the beam printed entirely with ferromagnetic composite material can obtain greater deformation.

The application of VP technology in magnetic sensing is still in its infancy, while, it shows greater application potential in magnetic-responsive actuations. However, there are still many gaps to be filled between the magnetic response and the magnetically controlled actuator capable of performing tasks, which will be further discussed in Section 4.5.

3.3. Moisture and pH Sensing

In the areas such as health, food quality control and environmental protection, there is a growing interest in the identification, quantification, and monitoring of common chemicals in daily life. Inexpensive and efficient are two highly desired demands, therefore, it is of great significance to develop simple and robust sensors with on-site features and further improve the sensing performance regardless of environmental fluctuations. There are many kinds of chemical sensors, while only moisture and pH sensors printed via VP are discussed

**ADVANCED
SCIENCE NEWS**

www.advancedsciencenews.com

**ADVANCED
MATERIALS
TECHNOLOGIES**

www.advmattechnol.de

in this section. More information about biochemical, gas, and particle sensing will be introduced in Section 3.4. A generally accepted principle of chemical sensor design is that they should detect substances and produce signals, such as color changes and fluorescence, which are easy to be measured.[106] Accordingly, Maldonado et al. used a thermo- and solvatochromic composite based on copper(II) 1D coordination polymer (CP1) with remarkable sensitivity, ranging from 0.3% to 4% of water in organic solvents.[107] By dispersing CP1 into biodegradable monomers to form the stable photocurable ink, different CP1 3D architectures that can detect moisture in air and solvents were printed, as shown in Figure 7c.

Furthermore, hydrogels are excellent candidates for chemical sensing as their ability to contain water and sensitivity to all kinds of external stimuli.[108] Depending on the density of charged groups, the swell/deswell behavior of hydrogels can be affected by the change of surrounding conditions, such as pH, organic solvent, temperature, light, and humidity.[109] Yin et al. presented the optical maskless stereolithography (OMsL) technology that can print 3D patterns of poly(acrylic acid) (PAA) hydrogel for miniature pH sensing, which has reference value for VP printing sensors with 3D structure.[110] The swelling degree of PAA ionic hydrogel increased significantly with the pH raised from 2 to 7. However, how to convert the unreadable volume changes into easy-to-read signals is a common problem faced by all hydrogel-based sensors. Figure 7d shows a schematic design of periodic PAA micropads forming a long-period grating as a miniature optical pH sensor. The pH was measured indirectly by measuring transmission spectra of the sensor with different lateral widths of PAA micropads. Three examples of PAA micropads were printed with different sizes patterned to encapsulate the microfiber and the high-resolution of OMsL ensure the encapsulation matched well.

Inspired by the humidity sensing of human hair, Li et al. developed electrical conductive composite hydrogels (PEGDA/MWCNT) capable of detecting chemical liquid, and build multifunctional flexible liquid sensors with multimaterial enabling anisotropic detection of microliquid droplets.[111] A mesh-shaped liquid sensor that can effectively identify the position and volume of liquid leakage in a short time, and a three-layered liquid sensor to enable bidirectional monitor and detection of the liquid leakage in two different sides were fabricated.

3.4. Microfluidic Device-Based Bio- and Particle Sensing

3.4.1. Microfluidic Devices

Microfluidic devices, which enable the precise routing of liquid streams and selectively control the tested particles,[112] as well as the flexible design of microreactors, precise control of reaction parameters, parallelization of thousands of reactions, and integration with feedback devices,[113] are ideal platforms for biological and inorganic particle sensing. Traditionally, microfluidic devices can be mass-produced by soft lithography,[114] microhot embossing,[115] and microinjection,[116] however, either a lack of diversity and versatility in testing or a lack of convenience and economy in prototyping, hinders the wider application of microfluidic devices.[117] 3D printing allows

the manufacturing of complex prototypes directly from computer-aided designs with few geometric constraints, resulting in increasing importance in microfluidic device manufacturing.[118] It also promotes the development of point-of-care testing, which means the medical diagnostic tests are available at the time and place of users rather than being inspected and analyzed in laboratories.[118–119] Also, the recent 3D-printed smartphone-based peripheral components for biosensing have proved the ability of 3D-printed devices in portability, multiplexing, and intelligent readout, which can meet the growing demand for home diagnostics, field analysis, real-time health or environmental monitoring.[117,120]

Compared to other existing 3D printing technologies, VP provides microfluidic devices better design freedom and surface quality.[121] Voids and channels can be printed into microscale with complex 3D structures (especially, the TPP technique promise substantially improved resolution (<10 μm) with a concomitant reduction in writing times and costs).[122] Functional elements, such as valves and pumps, can be precisely integrated into the device to ensure the control and direction of fluid flow.[123] Other structures such as microneedles with open microfluidic channels,[124] microfluidic modularized manufacturing,[125] printing microfluidic structures on surface-functionalized polymer substrates,[126] and 3D parallelized microfluidic droplet generators and microfluidic for automation of sequential liquid control were all achieved by VP as well.[127] These structures are usually modularized, so they can be easily and freely recombined for other applications. According to different detected objects, the application of VP technology in microfluidic device-based gas and flow particle sensors and biochemical sensors will be introduced, respectively.

3.4.2. Gas and Flow Particle Sensors

The separation of small-scaled particles from a gas or liquid media is an essential task for many biological and chemical analyses and environment quality assessments.[128] Based on precise manipulation of fluids and particles within microscale confinements, VP-printed microfluidic device-based separators can be used in solid–liquid and solid–gas separation to prepare for the subsequent further analysis. Accurate and rapid separation of abiotic particles, which have no related biological or chemical activity, can be simply achieved by physical methods and characterized according to their size, quantity, or concentration.

Inspired by hydrocyclone, a widely used particle separation technology in macroscale industrial processes, Han et al. developed a microscale hydrocyclone with critical feature size as small as 250 μm, which is able to separate particles as small as 3.7 μm, by taking advantages of 3D printing using SLA coupled with DLP.[129] VP breaks through the limitation of using traditional microfabrication technology to realize the internal helical structure of hydrocyclone and guarantee the separation performance of the device. **Figure 8**a shows a representative 3D-printed microfluidic device, which has a hydrodynamic focusing chamber with a focusing junction to achieve streams selectively passing through and realize the particle-by-particle counting.[130] With embedded optical fibers, the device has
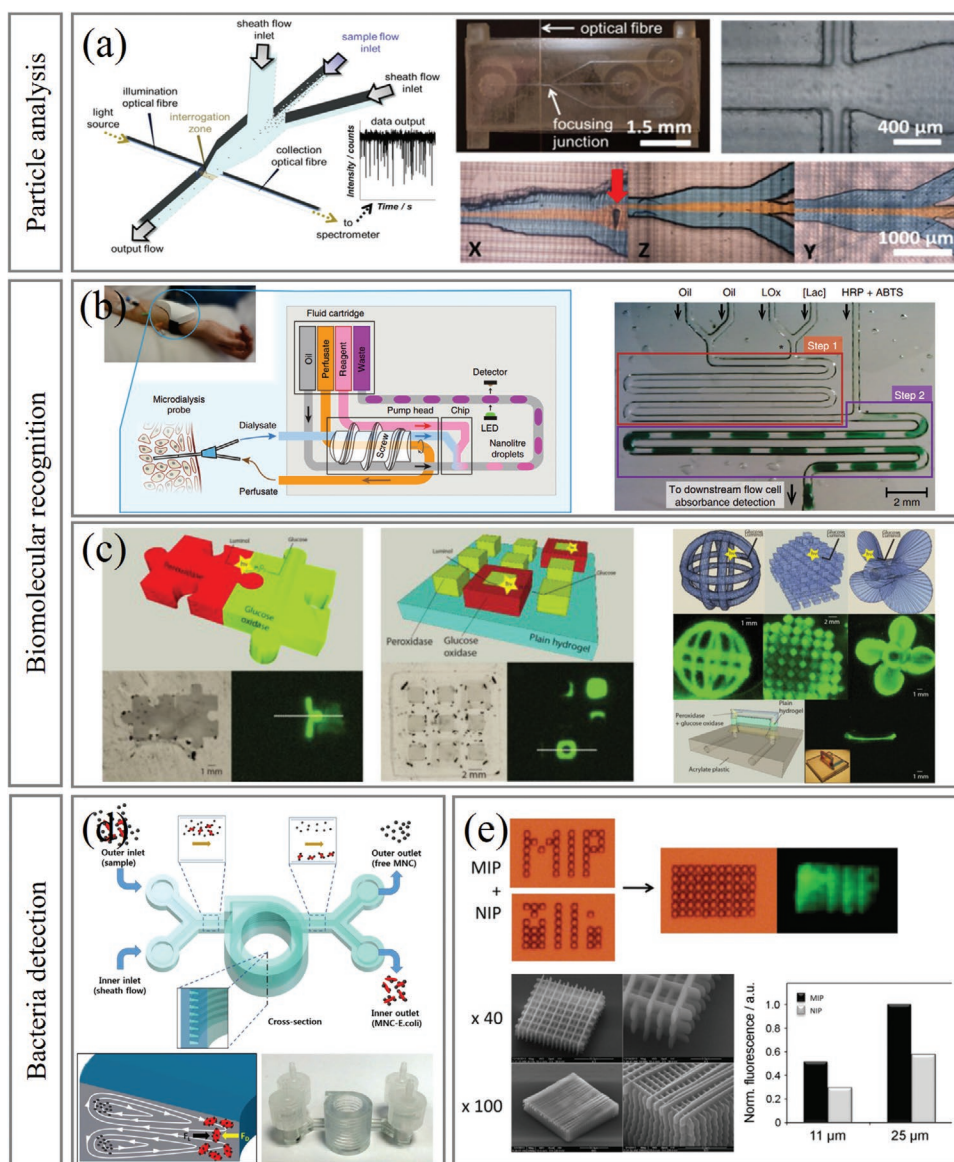
**ADVANCED
SCIENCE NEWS**

www.advancedsciencenews.com

**ADVANCED
MATERIALS
TECHNOLOGIES**

www.advmattechnol.de

Figure 8. VP-based microfluidic devices and applications in particle and biosensing. a) The 3D-printed device with hydrodynamic focusing and detection ability. Reproduced with permission.[130] Copyright 2018, Elsevier. b) The operation of the device with a droplet flow regime and a screw-driven push–pull peristaltic micropump (left), and the lactate assay being performed on-chip (right). Reproduced under the terms of the CC-BY Creative Commons Attribution 4.0 International License.[137] Copyright 2019, The Authors. Springer Nature. c) Directly printed sensing layer based on hydrogels entrapped with horseradish peroxidase or glucose oxidase. Reproduced with permission.[140] Copyright 2016, American Chemical Society. d) Working principle of the microfluidic device that can generate Dean vortices. Reproduced under the terms of the CC-BY Creative Commons Attribution 4.0 International License.[149] Copyright 2015, The Authors. Springer Nature. e) Specific recognition of the MIP and its potential in fabricating woodpile-type porous 3D microstructures. Reproduced with permission.[153] Copyright 2016, Wiley-VCH.

the potential to evolve toward specific measurements, such as the ability to distinguish between cells and particles.[130]

3.4.3. Biomolecular Sensors

Biochemical sensors refer to integrated devices that convert certain biological or chemical particles into a readable signal, such as optical and thermal changes, electrochemical reaction phenomenon, and mass-induced vibrations.[117] According to

different signal conversion principles, such biosensors can be divided into optical-based sensors, amperometric sensors, magnetic-based sensors, and resonance frequency variation-based sensors, etc. Because optical-based sensing is intuitive and easy to read, it is widely used in microfluidic devices as qualitative sensing,[118] while accurate quantitative perception is commonly achieved through the integration of electrochemistry or other kinds of systems.[131]

Depends on the chromogenic or luminescent reactions of biomolecules, VP-printed microfluidic devices can be used as

**ADVANCED
SCIENCE NEWS**

www.advancedsciencenews.com

**ADVANCED
MATERIALS
TECHNOLOGIES**

www.advmattechnol.de

biomolecular sensors to detect enzymes and DNA.[132] Bishop et al. demonstrated SLA-printed microfluidic devices with electrodes incorporated to detect phosphate buffer solutions and intact or damaged DNA by electrochemiluminescence (ECL) measurements.[133] For good transparency, the clear acrylate-based resin was employed, which allows the measurement of ECL generated by the reaction. Under certain conditions, the concentration of the core actants contained in DNA is linearly related to the ECL intensity. Tang et al. developed a rapid and sensitive microfluidic device, which can detect cancer biomarker protein through chemiluminescence.[134] With a programmable syringe pump and a charge-coupled device camera, the entire assay protocol can be automated. The high precision of SLA 3D printing ensures channel integrity and eliminates leakage of the microfluidic devices.

To sum up, the ability to integrate with electronics is important for microfluidic devices to realize automated control of more complex and flexible sequences of fluid movements, and more optimized integration strategies were indicated in recent papers.[118] Kadimisetty et al. also developed an automated system to evaluate the DNA damage instigated by environmental inputs like cigarette smoke by detecting ECL.[135] The microfluidic arrays have three sample chambers with microwells on the detection chip to facilitate reactions with enzyme/DNA films in the wells, and the damage degree of DNA is measured by ECL intensity. Similarly, Kadimisetty et al. reported another automated ECL array used for multiplexed detection of up to eight different proteins in human serum.[136] Using a sandwich assay design, the SLA-printed microfluidic cells introduce samples and reagents by passing them over a single-walled CNT that could then be activated to generate the ECL signal. Remarkably, the total cost of an array is reduced to $0.65 and eight-protein prostate cancer biomarkers in human serum samples can be detected within 25 min. Polyjet-based 3D printing also shows great potential in manufacturing highly integrated microfluidic devices with multiple functions. Nightingale et al. presented a microfluidic device act as a wearable sensor for monitoring biomolecule levels that combines continuous fluid sampling with in situ analysis using wet-chemical assays.[137] As shown in Figure 8b, a droplet flow regime and a screw-driven push–pull peristaltic micropump were integrated to form the fully autonomous and efficient detector. As a proof of concept, the lactate level in dermal tissue was tracked by the sensor and the result was in close agreement with standard off-line analysis and consistent with changes in peripheral blood levels.

Achieving direct printing of sensing materials instead of just cavities or channels, precision processing of biomaterials and other functional materials such as enzymes, antibodies, artificial catalysts, nanomaterials, and the development of resins with good biocompatibility are major challenges to be addressed. With the emerging of high-efficiency photoinitiators and high-absorbance photosensitizers, VP has become a promising alternative to process PDMS.[138] Hydrogels are another ideal biocompatible alternatives and it has been adopted to be microfluidic biomedical devices.[139] Using PEG-700-DA, a study reported by Mandon et al. preliminary confirmed the possibility of using DLP to produce hydrogel-based sensing layers with microstructures composed of enzymes and antibodies.[140]

A printed sensing layer containing glucose oxidase and peroxidase was printed and chemiluminescent signals were generated by a continuous enzyme reaction, as shown in Figure 8c. Except for that, models of fanciful ball, 3D pixel, and propeller were printed with entrapped peroxidase and glucose oxidase in the hydrogel. Propeller-like architectures were also fabricated as the sensing layers for the detection of brain natriuretic peptides. Besides, Chiadò et al. improved the immobilization of biorecognition elements by intrinsic functionality. Active moieties like carboxyl groups were introduced into different kinds of photocurable resin systems to print microfluidic devices for the detection of cancer angiogenesis biomarkers such as vascular endothelial growth factor and angiopoietin-2 by a colorimetric immunoassay.[141]

In addition to luminous reaction, Dirkzwager et al. developed a magnetic bead-based reactive colorimetric well diagnostic device for malaria by using SLA 3D printing.[142] By using the intrinsic enzymatic activity of a malaria biomarker, which generates a visible blue color in response to plasmodium positive samples, recombinant malaria biomarker at ng mL^{-1} concentrations using low sample volumes (20 µL) was successfully detected. Beauchamp et al. demonstrated a microfluidic device for detecting preterm birth biomarkers through electrophoresis separation.[143] SLA was used to print the microfluidic device with valves, pumps, chip-to-chip interconnects, and the preterm birth biomarker immunoaffinity capture structures with the minimum size characteristics of the channel up to 18 × 20 µm. Bertana et al. developed an electric-based dopamine biosensor made by 3D organic electrochemical transistors composite PEGDA:PEDOT resin.[144] The sensing material was printed directly and the sensing response is guaranteed by the good electrical conductance, bulk ionic diffusion mechanism, gating response in organic electrochemical transistors (OECTs) architectures of PEGDA:PEDOT. Compared with PEDOT:PSS, PEGDA:PEDOT OECTs showed an enhanced sensitivity of 0.41 V dec^{-1} toward dopamine detection.

3.4.4. Bacteria and Molecule Sensors

Traditionally, monitoring bacteria have several mature methods without cultivation, such as polymerase chain reaction,[145] electrochemical impedance spectroscopy,[146] fluorescence spectroscopy, and surface plasmon resonance.[147] For microfluidic devices, isolation and culture of the detected bacteria and molecules are two major applications.[148] The introduction of magnetic particles and a magnetic field for preconcentration is one solution for isolation. VP ensures the shape and size of the microchannels and an effective combination of magnetic particles and targets. Typically, Lee et al., presented an SLA 3D-printed microfluidic device for separating pathogenic bacteria, *Escherichia coli* captured from milk through inertial focusing.[149] Figure 8d shows the design of the device and the separation scheme for isolating magnetic nanoparticle clusters–*E. coli* complexes. Magnetic nanoparticles were attached to *E. coli* via antibody and act as capturer, and bacterial concentration was determined by bioluminescence measurements of adding adenosine triphosphate extracted from the bacteria to freeze-dried luciferin and luciferase powder.[149]

**ADVANCED
SCIENCE NEWS**

www.advancedsciencenews.com

**ADVANCED
MATERIALS
TECHNOLOGIES**

www.advmattechnol.de

The Dean vortices were generated as the fluid passes through a curved microchannel to separate particles into different sizes (Figure 8d).

Surface plasma resonance (SPR) spectroscopy based on plasma interface is a common method for no-label and real-time analysis and detection.[150] Relying on the good surface finish characteristics of VP, it is an ideal candidate for the manufacturing of optical components, notably high-quality, custom prisms for biosensing. Hinman et al. reported 3D-printed custom prisms that enable Kretschmann configured plasmonic sensing of bacterial toxins.[151] Equilateral prisms were printed via SLA with simple benchtop polishing procedures, and it was deposited with a gold layer as the plasmonic surface for a standard Kretschmann configuration setup. After attaching a tethered lipid bilayer and GM1 to capture cholera toxin, it was able to detect with good sensitivity. Gold nanoparticles were also grown on the surface of a dove prism via polydopamine for using in the single-axis configuration of SPR.[151]

Except for microfluidic device-based biochemical reactions, resonance measurement is a common physical method used in microcantilever-based mass-sensing, its high sensitivity to small mass objects is ideal for measuring particles, such as viruses, DNA, or nanoparticles.[152] VP provides technical support for miniaturization and refinement of the resonant mechanical structures. However, to achieve molecular recognition of cantilever beams, one challenge is to print the advanced functional material directly. Gomez et al. proposed a method of using TPP to create micro–nanostructured microbiosensors based on molecularly imprinted polymers, a biomaterial allowing the molecular recognition and binding of target analytes with a high affinity and specificity.[153] Figure 8e shows the molecular recognition ability of the printed microstructured MIP and indicates the possibility to create highly multiplexed biochip-like devices allowing the detection of several molecules on the same chip. The woodpile type porous 3D microstructures generated different fluorescence signals when binding with certain molecules, which shows good accessibility of the binding sites and the possibility to make a microcantilever-based sensing structure. Finally, the cantilever sensor including their clamped base was printed in a single step on a glass support. The resonance frequency is measured before and after the incubation of the analyte, and the concentration of the analyte was measured from relative frequency shift. What's more, Stassi et al. demonstrated a microcantilever with intrinsic functionalities for mass-sensing.[154] The device was prepared by an acrylic-based formulation with the addition of acrylic acid, which was able to selectively measure the incubations of the recombinant protein G and horseradish peroxidase-conjugated goat antimouse immunoglobulin G.

In conclusion, VP provides a faster, cheaper, and more accessible single-step procedure in manufacturing prototypes of microfluidic devices and microcantilever-based sensing structures. It can readily combine multiple components and processes in a single device. Currently, VP fabricated sensing elements or fully printed biosensors and bioanalytical devices are rare. Because the processing of sensing material normally depends on excellent printing conditions to ensure the biological activity of the material. Besides, the preparation of the sensing layer requires ultrafine printing resolution to ensure the reliability and stability of the sensors. While the development of photocurable hydrogel-based materials has demonstrated one possible solution, more importantly, its potential for other sensing and stimulus responses opens up the possibility of integrating multifunctional devices in the future.

4. Fabrication of Actuators via VP

Actuators, which refer to the devices that integrate stimuli-responsive materials with mechanisms to transduce external stimulus into motions,[155] are core elements for machines and robots. The stimuli can be heat,[156] water,[157] electric or magnetic field,[158] light,[159] etc. Yet, the pressure-driven actuators, represented by pneumatic and hydraulic actuators, are another common type, which can rapidly output high power, has the potential of lightweight and performs arbitrary deformation through constraint structural design.[160] However, the connection requirement of a large pump or compressor limits their operating scenarios. While the stimuli such as electric and magnetic fields allow for micrometer-scale miniaturization, being remotely controlled and rapidly modulated.[161] Light-induced actuation is usually applied in remote rapid response on a small scale as well, and it shows potential in energy harvesting, self-cleaning surfaces, sensors, and photocontrolled microfluidics.[162] Based on swell/deswell effect of hydrogels, moisture- or solvent-induced actuations can cause large volumetric changes, however, they are sensitive to the environment, usually isotropic and the response speed is highly dependent on changes in solution composition.[163] These actuators are more suitable for operating in fluids and precisely controlled environments, such as valves and pumps for microfluidic devices mentioned above. Among all the stimuli, the thermal stimulus is the most common one, and it can be converted from other stimuli to achieve localized stimulus, such as light or electricity.

In fact, the conventional actuators are confined by the simple uniform distribution of moments in a rigid body. They are often difficult to realize internal deformation and cannot meet the requirements of a safe human–machine interface.[161] In manufacturing soft actuators, the traditional manufacturing approaches, such as molding and soft lithography, require high precision, and the constraint structure is often designed to be a relatively simple geometric shape.[164] Recent advances in AM have introduced 4D printing,[165] in which, the shape, property, and functionality of a 3D-printed structure could evolve with time when it is exposed to a predetermined stimulus, providing new technical support for the development of actuators.[166] 4D printing originates from the development of 3D printers combined with printable smart materials, which refers to the functional polymers and nanocomposites that undergo structural changes upon exposure to external stimuli. Currently, 3D printing technologies, such as direct ink writing (DIW),[167] SLA,[168] inkjet printing,[169] and selective laser sintering (SLS)[170] are explored to achieve 4D printing by demonstrating the shape memory effect of structures.

The related smart materials also have been widely reported in the past decade, which include shape memory alloys (SMAs),[171] shape memory ceramics (SMCs),[172] shape memory

ADVANCED
SCIENCE NEWS
www.advancedsciencenews.com

ADVANCED
MATERIALS
TECHNOLOGIES
www.advmattechnol.de

polymers (SMPs)[173] and hydrogels,[108] dielectric elastomers,[174] and liquid crystal elastomers.[175]

With the emergence of novel photocurable smart materials, VP has made great progress in printing stimuli-responsive structures, and various functions are realized, including active origami, self-folding or self-assembly, self-healing, and other stimuli-based actuation.[17] Compared with SMAs and SMCs, SMPs and hydrogels are two major smart materials used in VP methods due to their printability, large deformation ability, alternative driving mechanisms, light weight, and low price.[176] With the high-resolution and highly free manufacturing capability for 3D structures, VP accelerates the miniaturization of actuators, besides, the emerging of biodegradable and biocompatible hydrogels show a promising application prospect in vivo. Furthermore, Polyjet can process multiple smart materials to achieve multishape memory effect and sequent actuations, especially in the case of manufacturing fiber-like, layered, and fabric structures without complex 3D structures.

The selection of response mechanism is critical for the application of soft actuators, because stimuli should be configured based on different scenarios. In Section 4, the recent progress of VP in actuator manufacturing, and other shape shifting structures and devices will be introduced according to the stimuli-responsive mechanisms.

4.1. Temperature-Induced Actuation

SMPs and hydrogels are two major thermal-responsive materials used in VP.[166] A SMP commonly consists of two relatively independent phases in its structure, which are the fixed phase and the reversible phase, respectively. The fixed phase determines the permanent shape and can be formed by physical or chemical crosslinks, while the reversible phase allows temporary shape deformation and shape recovery. The shape memory process of an SMP includes programming and shape recovery.[177] A typical deformation cycle of an SMP induced by temperature includes: 1) defining the temporary shape of SMP with applied external forces over T_{perm}, the temperature that must be exceeded, 2) keeping the external forces until the temperature drops down to the thermal transition temperature T_{trans} to set the shape (in some cases, T_{trans} could be the glass transition temperature T_g and others the melting temperature T_m), and 3) Raising the temperature above T_{trans} again and releases the internal stress, and restores the SMP to its permanent shape.[178]

Extrusion- and jet-based AM are relatively easier to print SMPs as they can process inks with both rigid parts and elastomeric parts by simply mixing two different materials. Furthermore, sequential complex shape change can be realized by the integration of different SMPs with discrete or reversible transitions.[27b,179] However, the poor mechanical properties and the immutable glass transition temperature impede such SMPs from being widely used.[180]

For VP, one challenge is keeping SMPs printable throughout the programming process. The resins typically used in VP are highly crosslinked thermoset polymers, and therefore the resultant parts are stiff and rigid with poor shape memory properties.[181] To generate shape memory effect in an SLA-printed part, Choong et al. introduced the *tert*-butyl acrylate-*co*-di(ethylene glycol) diacrylate network, which consists of a monomer with shorter chains that enable large plastic deformation into a temporary shape, as the soft component, and crosslinker with strong covalent bonds or intermolecular interactions with each other that remain thermally stable to define the permanent shape, as the hard component.[181] A shape memory C60 bucky ball with two temporary shapes is shown in **Figure 9**a, however, the insufficient stretchability (failure strain of 8.79% when temperatures below T_g and 18.2% when temperatures above T_g) prevents it from being used in further actuation applications. Also, the one-way shape change is irreversible, resulting in a requirement of reprogramming for reuse. Therefore, the development of two-way SMPs (which means the material can undergo a spontaneous reversible transformation between two shapes with alternating external conditions)[182] is of great significance for SMP used in actuator applications.[183] Zarek et al. demonstrated an SLA printer with a customized heated resin bath printing that can overcome the poor processing characteristics of thermosets and enables complex shape memory geometries.[15c] Polycaprolactone (PCL), a semicrystalline polymer, was covalently linked with methacrylate groups as the resin and heated to a molten state to be photopolymerized. Figure 9b shows a series of shape memory models, including a bird, an Eiffel Tower, and a temperature-controlled reversible electric switch with conductivity obtained by inkjet-printed silver nanoparticles. When PCL is co-crosslinked with 2-ureido-4[1*H*]-pyrimidinone (UPy) units, which contains multiple hydrogen bonding interactions and reversible intermolecular crosslinks, it can be used to print self-healing and shape memory structures. Invernizzi et al. developed such a polymer (PCLDMA/UPyMA) to realize thermally triggered self-healing and shape memory at the same time.[70] However, only ≈50% of its original tensile strength and ≈20% of its original failure strain were recovered after healing and the printed structure stayed in the only 2D. Based on that, Zhang et al. used PCL as the self-healing agent, benzyl methacrylate as the chain builder and poly(ethylene glycol)-dimethacrylate as the crosslinker to prepare a highly deformable and 3D printable SMP network with self-healing and shape memory abilities.[184] The high-resolution (up to 30 μm) of DLP was fully utilized that grippers and stents were printed and the mechanical properties of a damaged structure can be recovered to more than 90%.

In order to develop an SMP with further improved toughness, shape recovery ratios and permanent shape reconfiguration, Miao et al. created dynamic imine bonds between monomers and crosslinker in the SMP networks.[185] Smart devices such as aerospace structures, soft robotic grippers, smart electron switches, and intelligent packaging were printed and the reconfigurability of this SMP shows an expanded application scope of 4D printing materials. Epoxy resin is another thermoset resin that can be developed for shape memory applications.[179a] By controlling the crosslink density, shape memory epoxy resins can be printed with improved toughness and good shape memory properties. Yu et al. used an epoxy-acrylate hybrid photopolymer to print shape memory 3D structures that show good mechanical properties, including high strength and good toughness due to the composition and structure of the hybrid photopolymer.[186] To achieve higher tailorable SMP thermomechanical properties, Ge et al. presented a PμSL-based
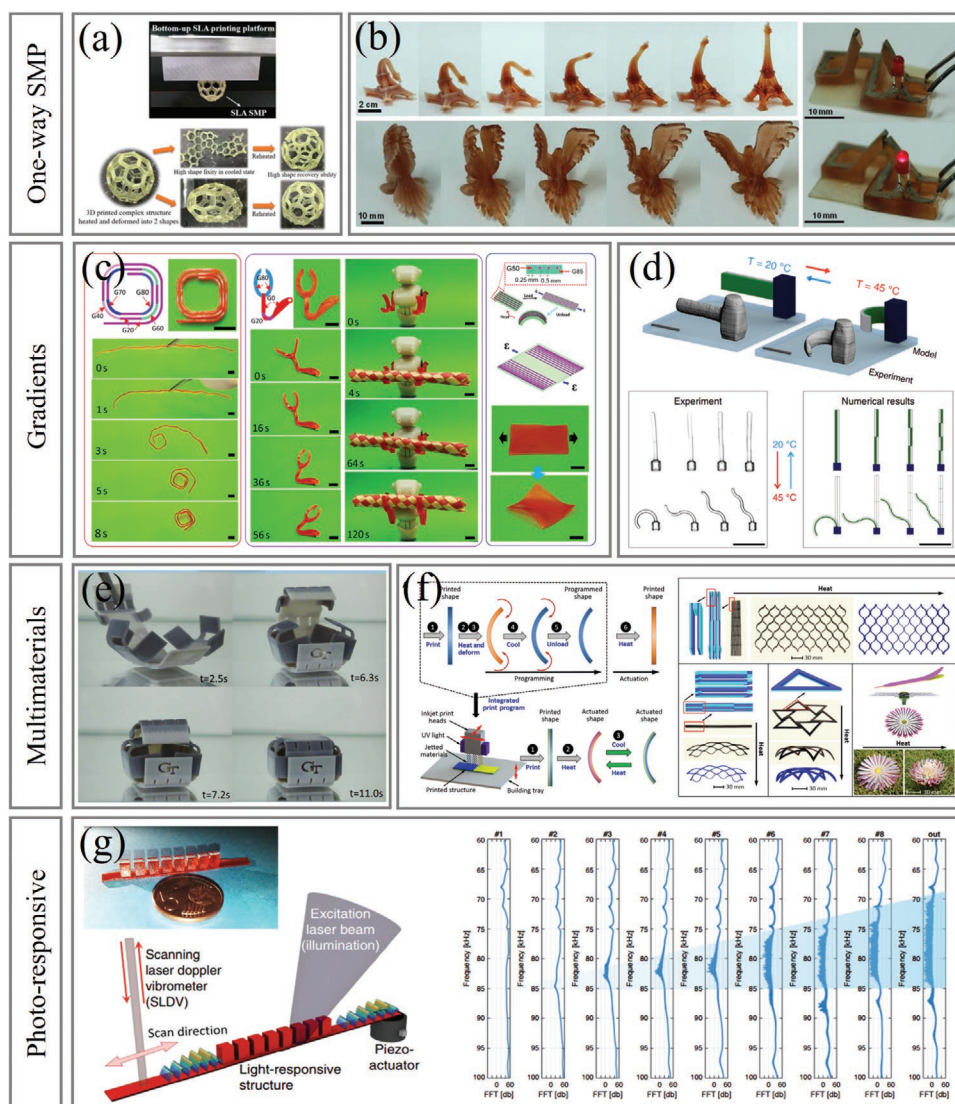
**ADVANCED
SCIENCE NEWS**

www.advancedsciencenews.com

**ADVANCED
MATERIALS
TECHNOLOGIES**

www.advmattechnol.de

Figure 9. VP-based temperature- or light-induced shape memory structures and Polyjet-based multimaterials shape memory structures. a) The temperature-induced shape memory ball with two temporary shapes. Reproduced with permission.[181] Copyright 2017, Elsevier. b) SLA-printed molten macromethacrylate-based shape memory model in any shape (left), and a shape memory electric switch (right). Reproduced with permission.[15c] Copyright 2016, Wiley-VCH. c) Sequential SMP components and 4D printing with gradient by grayscale DLP. Reproduced under the terms of the Creative Commons Attribution NonCommercial License 4.0 CC BY-NC[191] Copyright 2019, The Authors, AAAS. d) Bimaterial heterostructures to realize temperature-induced directional actuation (top), and the experimental and numerical results of complex actuation (bottom). Reproduced under the terms of the CC-BY Creative Commons Attribution 4.0 International License.[200] Copyright 2019, The Authors. Springer Nature. e) A self-folding box printed by Polyjet. Reproduced under the terms of the CC-BY Creative Commons Attribution 4.0 International License.[180] Copyright 2015, The Authors. Springer Nature. f) Comparison between SMP-based 4D printing and the direct 4D printing approach (left), and its application in printing structures consisting of multiple elements (right). Reproduced under the terms of the Creative Commons Attribution NonCommercial License 4.0 CC BY-NC[179b] Copyright 2017, The Authors, AAAS. g) Picture of the light-responsive metamaterial (left), and its spectral response without illumination (right). Reproduced under the terms of the Creative Commons Attribution 4.0 International License.[205] Copyright 2020, The Authors. Springer Nature.

4D printing method that can create SMP architectures with rubbery modulus from 1 to 100 MPa, T_g from −50 to 180 °C, and the failure strain up to 300% by using benzyl methacrylate and several difunctional acrylate oligomers.[187] A series of multimaterial grippers and flowers were manufactured through a multi-vat approach, which enables the materials to be placed at different positions to realize the reversible shape change of grippers.

Triple and multiple SMPs, which refer to the SMPs that have three or more temporary shapes, are achieved based on the incorporation of a broad thermal transition range into the polymer or the introduction of two or more discrete thermal transitions into the polymer.[188] The significance of multiple SMPs can be reflected in the work done by Peng et al., who formulated an acrylic acid-based photocurable triple SMP and fabricated flowers and microfluidic devices by a DLP printer.[189]

**ADVANCED
SCIENCE NEWS**
www.advancedsciencenews.com

**ADVANCED
MATERIALS
TECHNOLOGIES**
www.advmattechnol.de

The shape change of the flower can be programmed in three ways, which means the petals can open in different orders controlled by the temperature, and the nozzle of the microfluidic device can be placed in three grooves at different temperatures. For another example, Inverardi et al. used a commercially available resin (Clear FLGPCL02) with a broad glass transition to realize a multiple and sequential recovery, and a self-locking clamp was printed according to the triple shape changing effect of this SMP.[190] Based on that, grayscale DLP 3D printing for materials with widely tunable mechanical property gradients achieves the printing of multiple SMPs with heterostructure. Kuang et al. introduced a two-stage curing hybrid ink system to obtain functionally graded materials with a mechanical gradient up to three orders of magnitude and high-resolution.[191] Depending on the tunable grayscale level from G20 to G80, a series of sequential shape change structures were realized, such as a helical sequentially curved hinge, an artificial arm and a film with asymmetric fiber distribution, as shown in Figure 9c.

Compared with SMPs, hydrogels have significant mechanical strength disadvantages and the actuation of hydrogels is essentially driven by water swelling and shrinkage, thus, the response speed is relatively slow and the shape change is not stable. However, the water retention of hydrogels is often sensitive to various external stimuli, of which temperature is the most common one.[192]

The homogeneous structure can only make the hydrogel actuator achieve simple uniform expansion/contraction under the uniform stimulus, while the expected actuations are typically inhomogeneous, which occurs at different magnitudes in different directions. The ambient temperature rise around hydrogels is usually uniform, while the nonuniform temperature control is usually achieved by indirect heating, such as Joule heating,[193] photothermal effect,[194] and hysteresis effect,[171] as well as remotely controlled by a magnetic field.[195]

Another method to achieve the anisotropic deformation relies on the fabrication of asymmetrical distribution in material properties, composition, or microstructure across the hydrogel.[196] VP provides easy access to each individual building layer during fabrication and gives absolute spatial control over material placement and structure creation over the entire process,[196] so that the actuators can perform motions more accurately. Ji et al. arranged microstructures (parallel grooves) on the side of hydrogel strips, resulting in the bending or twisting deformations due to the asymmetrical swelling, to perform various complex deformations.[197] A thermal-responsive, water temperature controlled shaping-morphing gripper was printed and applied for transporting a hollowed ball. Such kind of structural design is also commonly used in pneumatic and hydraulic actuators, which will be introduced in Section 4.6.

N-isopropylacrylamide (NIPAM)-based hydrogels are one of the most appropriate hydrogels for soft actuators as they can be hydrophobic and expel water when the temperature is only slightly elevated above its lower critical solution temperature.[198] According to this characteristic, Han et al. developed the poly(*N*-isopropylacrylamide) (pNIPAM) hydrogel with microstructures via PµSL and realized virtual bilayer beam with different swelling characteristics by controlling the light intensity.[199] A gripper consisting of four beams was fabricated using two different grayscale levels. The difference in the swelling ratio between the two regions caused the bend of the beam toward the center at high temperature. A dumbbell-shaped structure was also printed, half of which was joined by an ionic monomer, causing the local shrinkage as the temperature rose. Similarly, Hippler et al. introduced pNIPAM-based bimaterial hetero-microstructures that exhibit complex actuation responses, which are in good agreement with numerical predictions, as shown in Figure 9d.[200] By controlling the intensity of light, the so-called gray-tone lithography approach of TPP, a highly localized control over the crosslinking density and consequently of the thermoresponse of the structure was achieved, and the minimum feature size is less than 30 µm.

Shiblee et al. developed poly(dimethyl acrylamide-*co*-stearyl acrylate and/or lauryl acrylate) (PDMAAm-*co*-SA and/or LA)-based shape memory hydrogel, which has tunable mechanical properties, by adjusting the concentrations of the crystalline monomer SA or LA.[15a] A customized 3D printer was used to print a macroscopic soft gripper with a bilayer structure via multi-vat 3D printing.[201]

Compared with the multi-vat approach of VP, Polyjet-based multimaterial printing is a more convenient alternative for processing photocurable materials. A typical work studied by Mao et al. demonstrated a so-called digital SMP printing which achieved a sequenced folding of a hinge structure under a spatially uniform temperature field.[180] Two base materials, VeroWhite and TangoBlack, were mixed at specific ratios to achieve prescribed thermomechanical and shape memory behaviors so that printing parts can change their shape in sequence without self-collision by adjusting the proportion. By using this strategy, a 3D folding box was successively made, as shown in Figure 9e. Ding et al. proposed a direct 4D printing method using SMPs to integrate programming into the printing process, which means that the sample can change its shape immediately after printing without any composition change required by gel-based 4D printing or the thermomechanical training required by SMP-based 4D printing.[179b] As Figure 9f shows, it integrates five separate printing and programming steps into a single one. As a proof of concept, lattice structures, flat star-shaped structures, and flowers consisting of multiple petals were printed with flexibility offered through the combination of geometrical, material, and processing design parameters.

4.2. Light-Induced Actuation

When exposed to specific wavelengths, photoresponsive materials can be triggered for a reversible photomechanical actuation mainly in two ways: photothermal effect[202] and photochemical effect.[203] In the photothermal case, the presence of an ideal absorber, which absorbs light and converts the energy into heat, can trigger actuations while avoiding thermal lag, thermal diffusion, and nonuniform heat distribution. While the photochemical effect is based on photoreactions of light-sensitive groups, such as photoisomerization and photodimerization.[159] In this case, a chemical reaction is used to power and control mechanical motion.[159] Limited by the mechanisms, the photoresponsive actuators can only perform tasks at a small scale commonly.

In the presence of near-infrared light, the forced resonance vibration process in the photon–phonon interaction

**ADVANCED
SCIENCE NEWS**

www.advancedsciencenews.com

**ADVANCED
MATERIALS
TECHNOLOGIES**

www.advmattechnol.de

of graphene can increase the degree of disorder and generate thermal kinetic energy.[204] Inspired by this mechanism, Lyu et al. developed photothermally responsive composites produced by reduced graphene oxide-filled chitosan-methacrylamide (rGO–chitosan-MA) patterned on thiolated PDMS substrates.[204] The so-called maskless DLP technology was used to print a bilayered structure with gradient rGO–chitosan-MA thicknesses(2–8 µm) by controlling the light intensity.[204] Self-rolling and self-folding structures, a "walking worm" structure and a kirigami-inspired flower structure were printed as a proof of concept. With a similar structure design scheme, bimaterial hetero-microstructures by controlling the intensity of light, Hippler et al. used photoinitiator Irgacure-819 in the pNIPAM-based network as the light absorber and realized two-photon absorption induced local bending at a fast speed.[200]

Azopolymers are well-known molecular photoswitches whose photoisomerization process constitutes the underlying mechanism for many photoinduced effects including mechanical photoactuation.[205] Polymers containing azobenzene units have been reported to be used in VP methods to produce photoresponsive devices recently. Aromatic azo compounds usually have relatively stable trans structures, unless when the appropriate wavelength of light is irradiated, the trans structure will gradually transform into a *cis* structure, and it is reversible when irradiated by visible light.[206] By using this photoisomerization process, many photoinduced effects, such as photofluidization,[207] mass migration,[208] tuning of elastic modulus[209] or wettability,[210] and mechanical photoactuation can be achieved.[205] Roppolo et al. introduced azobenzene compounds within photocurable polymer formulations and achieve accurate DLP 3D printing of crosslinked matrices.[211] Under laser irradiation, the softening and hardening can occur depending on the T_g of the polymer matrix and the operating temperature. In addition, Gliozzi et al. fabricated a light-responsive elastic metamaterial waveguide by using methyl red as azo-dopant to determine the tuned transmission spectrum of the metamaterial through the light field.[205] The Young's modulus of the metamaterial can be reduced due to the photoisomerization of the azo-unit, resulting in a corresponding modification of the finite waveguide elastic response of the metamaterial and the overall metamaterial band gap can be significantly widened under a local illumination (Figure 9g). It can be used as an elastic-switch functionality with a 1 min lag time and the light response components such as beam splitters, switches, and filters can bring substantial improvements to active elasto-wave-controlled devices.[205]

Photoresponsive smart materials applied in biological lab-on-a-chip technologies and microfluidic systems provide a possibility to realize precise control, such as the delivery of ultralow-volume sample aliquots to precise locales and isolation, patterning and harvest of microscopic populations of cells for molecular characterization.[212] Other stimuli such as pH and ion often require large shifts, both of which may have a deleterious, and potentially prohibitive, impact on the function of microdevices (e.g., microfluidic platforms) and viability be fabricated into light-responsive functional cell enclosures by multiphoton photolithography.[212] Based on the light-triggered photoexpansion and photocontraction, these photoresponsive protein microarchitectures were used to capture, "farm," and release small populations of microorganisms.

4.3. Moisture- or Solvent-Induced Actuation

Moisture- or solvent-induced actuation does not require any artificial source of active energy, but utilizing the humidity gradient of the environment to drive the actuator. There are three main mechanisms associated with moisture-responsive materials: the plastic effect, in which the absorption of water decreases the T_g level of the material, leading to a shape change,[213] the breaking and reforming of hydrogen bonds induced T_g reduction,[214] and the swell/deswell effect of hydrogels as mentioned in Section 3.3.[215] There is no doubt that hydrogels are one of the most effective materials to respond to changes in water content. Their ability to expand in the presence of water can be precisely adjusted and the above-mentioned methods for directionality shape change, such as the introduction of asymmetrical distribution in material properties, composition, and microstructure design are still valid in this type. Zhao et al. demonstrated a bilayer water-responsive structure consists of hydrophilic PEGDA as the expansion part and hydrophobic poly(propylene glycol)dimethacrylate as the rigid part,[216] resulting in directional bending in water. Both materials are photocurable and thus can easily be patterned to complex shapes by using DLP (e.g., flower structure as **Figure 10**a shows).

By controlling the light irradiation intensity during the photopolymerization of hydrogels, a gradient of crosslinking density within a layer can be created.[15b]

Huang et al. demonstrated a digital printing device and created hydrogels with 2D gradient structures by adjusting exposure time to achieve different crosslinking densities.[15b] As Figure 10b shows, the swelling effect transformed the printed flat sheet into a 3D round cap.

When the cured hydrogels are immersed in ethanol for rinsing, uncured monomers in the less irradiated portion will diffuse out and leave behind loose spaces in the network.[168] Small solvent molecules can then infiltrate the loose network of hydrogels, increasing the volume of the hydrogels. While after drying, the so-called desolvation effect occurs, which can inverse this process and achieve a reversible shape change.[217] Benefiting from VP, local insufficient curing can be achieved more accurately and structures such as cartoon face mask, theater,[15b] flowers,[218] origamis, and grippers[219] were applied in solvent-induced inhomogeneous expansion and contraction. Figure 10c depicts an SLA-based 4D printing system developed by Miao et al., who investigated the autonomous and reversible shape change induced by desolvation.[218a] The printed structures changed shape in ethanol and recovered in water reversibly. From planar structure to structures with 3D characteristics, Zhao et al. developed a photocurable PEGDA-based hydrogel and created desolvation-induced shape change structures by selective exposure.[219] Origami (Figure 10d), bending structures, self-folding structures and a solvent-assisted gripper were realized. Also by desolvation-induced deformation, Han et al. presented a miniaturized needle with backward-facing barbs (200 µm wide) for drug delivery, biofluid, collection, and biosensing with improved tissue adhesion, as shown in Figure 9e.[168]

In addition, Jin et al. developed a set of heterogeneous stimulus-responsive hydrogels that can be printed into arbitrary 3D shapes with sub-micrometer features by TPP.[220] Various deformation-amplified mechanisms were achieved by programming
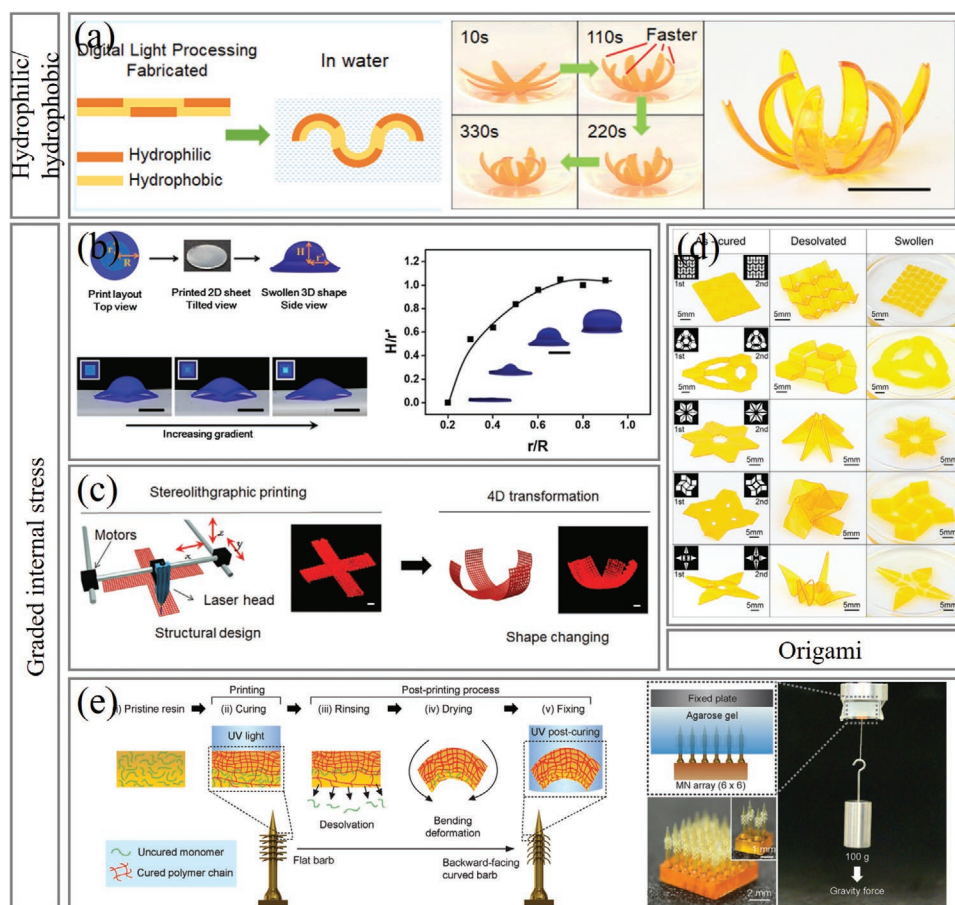
**ADVANCED
SCIENCE NEWS**

www.advancedsciencenews.com

**ADVANCED
MATERIALS
TECHNOLOGIES**

www.advmattechnol.de

Figure 10. VP-based moisture- or solvent-responsive actuators. a) The hydrophilic/hydrophobic composite structures to achieve complex bending. Reproduced with permission.[216] Copyright 2018, American Chemical Society. b) The gradient 2D hydrogel structure that is able to transform into a 3D structure by swelling effect. Reproduced with permission.[15b] Copyright 2017, Wiley-VCH. c) Schematic illustration of the stereolithographic printing process (left), and the desolvation-driven claw architecture (right). Reproduced with permission.[218a] Copyright 2018, Wiley-VCH. d) Desolvation-induced origami structures. Reproduced with permission.[219] Copyright 2017, Wiley-VCH. e) The process to program deformation of horizontally printed barbs into the backward-facing shape (left), and the strong tissue adhesion ability of the microneedle array. Reproduced with permission.[168] Copyright 2020, Wiley-VCH.

the exposure dosage of femtosecond laser pulses to create hydrogels distributed with different crosslinking densities, stiffnesses, and swelling/shrinking degrees.[220]

4.4. Electricity-Induced Actuation

In addition to inducing directional actuation in the form of joule heat,[14c] electric field can also induce electrochemical actuation directly. Compared with the former two types, electric stimulus is easy to accurately and rapidly adjust the magnitude, phase, and frequency, achieving immediate and reversible response.[161] Polymers and gels that are able to convert electrical energy into mechanical energy include conductive polymers,[221] liquid-crystalline elastomer,[222] and CNTs.[223] Among them, electroactive hydrogel (EAH) is commonly used for the preparation of VP-based actuators due to its bionic properties and processability.

Han et al. developed an EAH consists of AA as a monomer and PEGDA 700 as a crosslinker, which has large deformation

in electrolytes under the electric field.[224] According to Flory's theory and Donnan equilibrium, bending of the EAH can be caused by the motion of ions, which can induce osmotic pressure difference. The balance of which can be broken by the applied external electric field, resulting in nonuniform swelling between the interfaces, which causes the EAH bending toward the cathode.[224] Relies on the high-resolution of PµSL, an EAH-based gripper and a transporter were achieved as shown in **Figure 11**a.

The classic bilayer heterostructure is still feasible in electric-responsive actuation to acquire directivity. Han et al. developed a rapid multimaterial projection microstereolithography using dynamic fluidic control of multiple liquid photopolymers within an integrated fluidic cell.[225] A bilayer hydrogel beam consisting of hydrogels with different swelling properties under an electric field is shown in Figure 11b. Various modes and degrees of bending deformation were also realized by combining applied stimuli simultaneously (Figure 11b). Kang et al. proposed a poly(3-sulfopropyl acrylate, potassium salt)-based EAH with a mechanically enhancing multileg long-chain
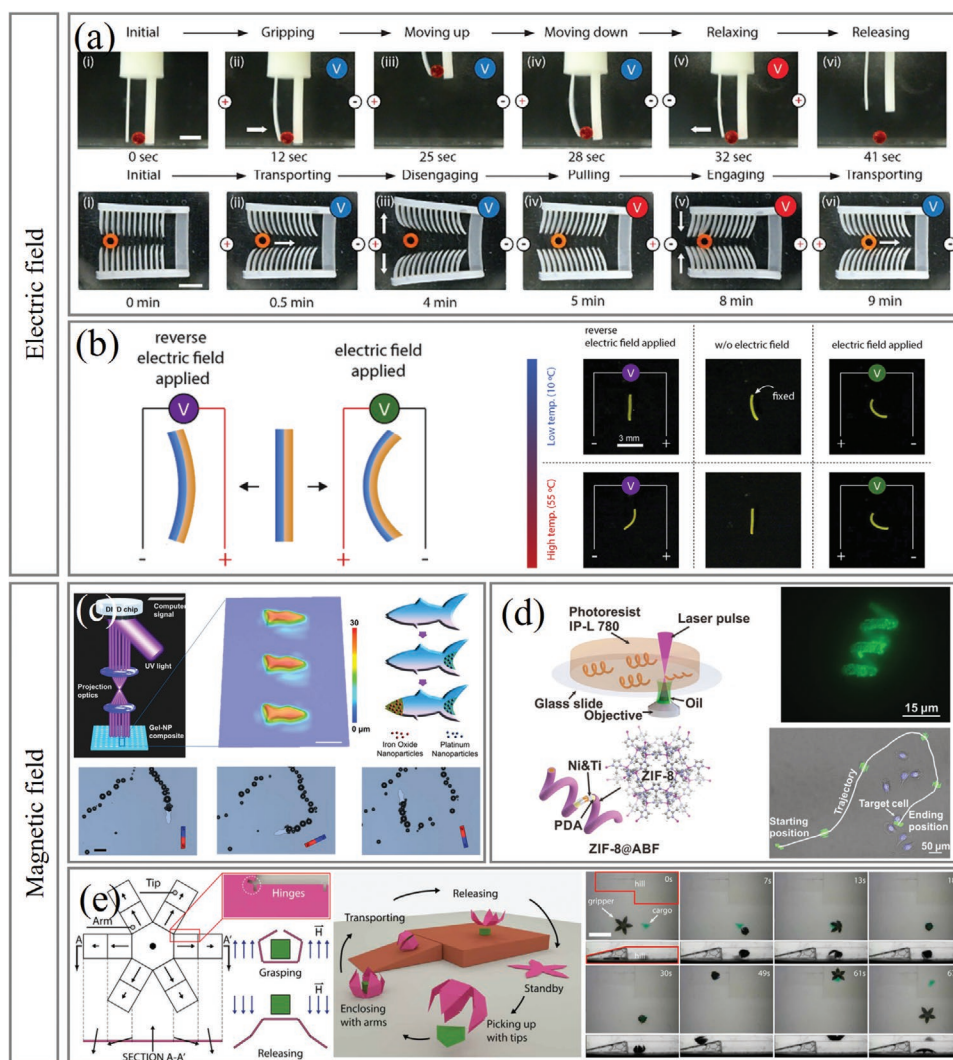
Figure 11. VP-based electric field- or magnetic field-driven actuators. a) Two kinds of soft actuators with 3D-printed EAH driven by electric fields. Reproduced with permission.[224] Copyright 2018, American Chemical Society. b) Bilayer hydrogel beam printed by the electroactive hydrogels (left), and its various modes and degrees of bending deformation (right). Reproduced with permission.[225] Copyright 2019, Elsevier. c) The microfish with Fe_3O_4 and Pt nanoparticles printed via μCOP method (top), and its moving ability driven by a rotating magnet (bottom). Reproduced with permission.[228] Copyright 2015, Wiley-VCH. d) The manufacture, fluorescence image, and the movement of ZIF-8@ABF microrobots. Reproduced with permission.[230] Copyright 2019, Wiley-VCH. e) Geometry, magnetization profile, and working mechanism of the magnetic microgripper (left), and the illustration and images of the cargo transportation task (right). Reproduced with permission.[231] Copyright 2019, AAAS.

crosslinker, glycidyl methacrylated hyaluronic acid, effectively address the limitations of hydrogel brittleness and the inability to carry out large-scale 3D printing.[226]

4.5. Magnetism-Induced Actuation

The magnetic field is another stimulus that can realize remote actuation and wireless control of devices. Introducing magnetic fillers into flexible photocurable resins or loading magnetic particles onto printed structures by surface functionalization process are common methods for VP to manufacture magnetic actuators. When these actuators are subjected to an external magnetic field, the magnetic particles in them will try to align with the field. Therefore, actuations such as torque,

deformation, contraction, extension and bending can occur under the influence of the magnetic force. Different actuation modes of these actuators can be designed by varying the magnetic field, magnetization properties, and the overall structure of the actuator. Besides, magnetic-driven actuators are ideal candidates for working in confined spaces because of their good penetration toward a lot of media.[227]

Zhu et al. demonstrated a DLP-based novel 3D-printed technology called microscale continuous optical printing (μCOP) and fabricated hydrogel-based freely swimming microfish structures (about 30 μm high and 120 μm long).[228] By replacing solutions, Pt nanoparticles were loaded into the tail of a fish for propulsion, and Fe_3O_4 nanoparticles were loaded into the head of the fish for direction, as shown in Figure 11c. The time-lapse images of the microfish's movement in 15% H_2O_2 clearly

**ADVANCED
SCIENCE NEWS**
www.advancedsciencenews.com

**ADVANCED
MATERIALS
TECHNOLOGIES**
www.advmattechnol.de

show the remote guidance ability of the microfish by rotating a nearby magnet. While μCOP in this example is limited to pattern 2D structure on a relatively flat surface, which cannot meet the requirement of manufacturing 3D magnetic-responsive actuators with complex structure.

Through TPP, the magnetically driven actuators can be created as micro- or nanorobots for future biomedical applications, such as diagnostics and drug delivery. The development of biocompatible and biodegradable materials and their magnetic properties are important. Wang et al. reported a magnetically driven transient soft microswimmer (with a length of 30 μm, a radius of cylindrical cross-section of 1.5 μm) made by gelatin methacryloyl, a versatile photocrosslinkable hydrogel with high cytocompatibility and bioactivity. The microswimmer has a helical structure and is obtained magnetic by incubated in aqueous suspensions of Fe_3O_4 nanoparticles. As a motile platform, it exhibits a unique swimming behavior under rotational magnetic fields and it can support cell adhesion, and growth, moreover, it can be gradually digested by cell-released enzymes during culture.[229] Similarly, they developed another magnetic-driven helical-shaped microswimmer (with a helical diameter of around 10 μm, a filament diameter of ≈3 μm) coated with a zinc-based metal–organic framework, zeolitic imidazole framework-8, which has magnetic property, high biocompatibility, and pH-responsive ability, as shown in Figure 11d. Therefore, controlled by external magnetic fields, it can be used as a pH-responsive targeted drug delivery platform to carry and release drugs. The complex trajectories can be followed by this swimmer within microfluidic channels.[230]

However, due to the lack of suitable materials and manufacturing technology, the construction of 3D structures with high deformation degrees of freedom on such small scales is faced with challenges. To solve these problems, Xu et al. reported a method for patterning permanent magnetic microparticles in an elastomer matrix to realized complex 3D shape transformation and locomotion.[231] Figure 11e shows a magnetically actuated six-degree-of-freedom microgripper (with the geometrical feature size as small as 100 μm), which exhibits higher-order, multiaxis bending, large-angle bending, and combined bending and torsion ability. In addition, for biocompatibility, the magnetic particles were securely encased by cured polymer composites to avoid contact with the biological tissue.

4.6. Pneumatic and Hydraulic Actuation

Pneumatic or hydraulic actuation is obtained through the dynamic reconfiguration of gas or liquid within a chamber made of highly deformable materials. These actuators enable fast response, maintain compliance at cold temperatures,[232] and generate high forces with the existence of the external pump or compressor.[233] Both the structure of the chamber that facilitates fluid flow and the material used to fabricate affect the performance of the actuators, especially, the appropriate geometrically asymmetric structures and anisotropic materials can cause the inflation of the chamber can be converted into a directional deformation of the whole actuator.[233]

Pneumatic and hydraulic actuators are commonly used for mesoscale functions, which require relatively low precision,

thus molding and soft lithography are feasible manufacturing options and are favored by commercial mass production. All kinds of commercial liquid elastic materials can be used to meet the requirements of various physical, chemical and mechanical properties (such as compliance, extensibility, and resilience),[234] and inextensible fibers can be added to further modify local stiffness and actuation profiles of the actuator.[235] However, VP methods avoid tedious and time-consuming iterative processing or assembly steps during integration. More importantly, it enables the creation of highly complex microscale voids and channels with ≈20 μm as mentioned in Section 3, resulting in more miniaturized and versatile actuators for more elaborate tasks.[236] To manufacture actuators directly, the development of photocurable elastic resins that are comparable to commercial elastomers is crucial. Patel et al. introduced a highly stretchable (the maximum amount of stretch reaches 1100%) and UV curable elastomer resin system consisting of EAA and AUD.[50] The tunable mechanical property can be achieved by adjusting the ratio of the two mixtures, which means a broader application scenario. As a proof of concept, soft pneumatic actuators were printed which can bear the local strain up to 170%.

For such gripper-type actuators, both flexibility and rigidity are indispensable as they can provide conformal and enough pressure to grab objects, respectively. Hence the mutually exclusive problem of strength and toughness becomes a classic materials-design problem. Inspired by nature, the tunable structural stiffness, achieved by multimaterial printing, allows a decentralized control of the actuators and improves its capabilities and efficiency.[237] Zhang et al. presented a generic process flow for systematic and efficient tailoring of the material formulation and key processing parameters for DLP.[164] The multivat approach was adopted to print an assortment of miniature soft pneumatic grippers with various structures and morphing modes, as shown in **Figure 12**a. Remarkably, debris removal in a confined space was achieved by combining a miniature soft pneumatic gripper and a continuum manipulator. Thrasher et al. reported a series of resins with adjustable components and mechanical properties.[238] By using the stratification of resins with different densities in the vat, the build stage was positioned just above the liquid–liquid interface, which defined the upper and lower boundaries of the build layer, respectively, enabling multimaterial printing. A pneumatic gripper was printed with a three-layer structure, which caused the differential strain of the gripper to enhance actuation efficiency. By developing a resin containing thiol–ene and condensation precursors, Wallin et al. created a kind of silicone double networks which simultaneously possess low elastic moduli (100 kPa < E100% < 670 kPa) and high elongation ($dL/L0 ≈ 400\%$), toughness ($U > 1\,MJ\,m^{-3}$), and strength ($\sigma ≈ 1\,MPa$).[239] More importantly, the printed objects exhibited excellent ability to integrate with other materials since the latent condensation reaction permits cohesive bonding of printed objects to dissimilar substrates with modulus gradients that span more than seven orders of magnitude.[239] Taking advantage of that, an elastomer-textile-based orthotic glove, and a bellows actuator integrated with the printed circuit board containing temperature-sensitive LEDs were fabricated.

Different from pneumatic actuators, fluid selection in hydraulic actuators is stricter to ensure their chemical inertia,
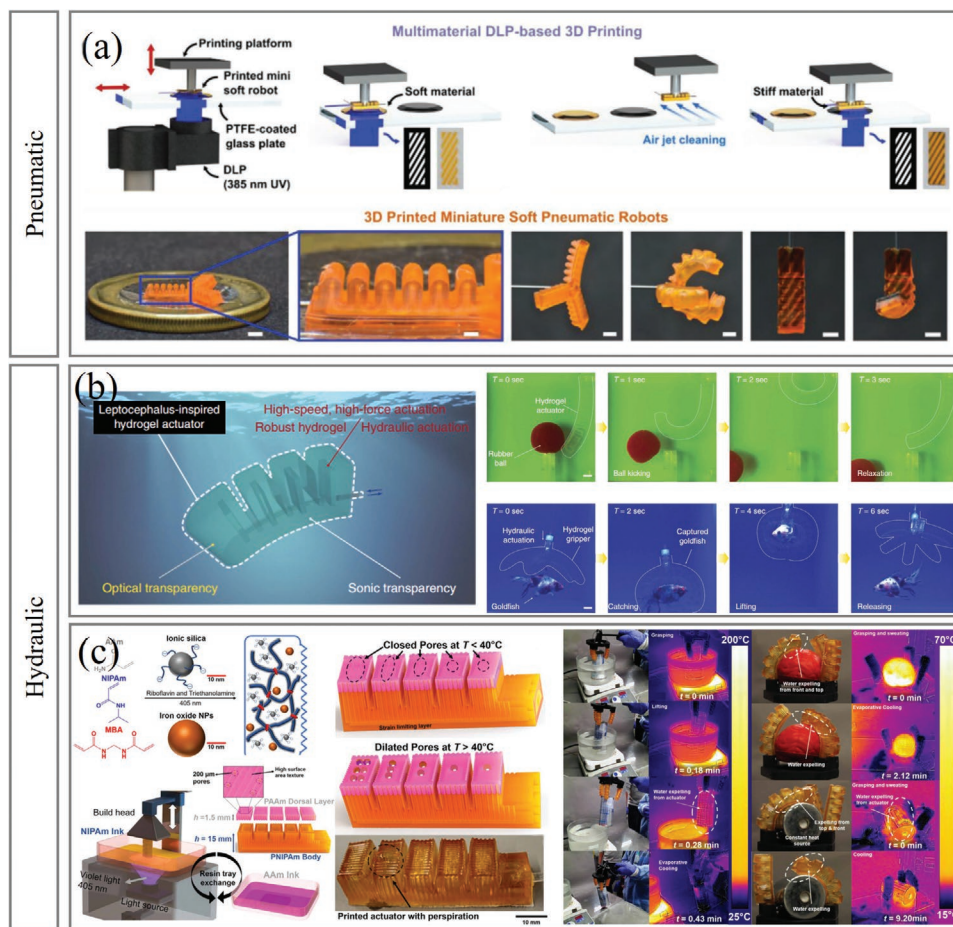
Figure 12. VP-based pneumatic and hydraulic actuators. a) Schematic illustrations of the self-built DLP-based multimaterial 3D printing system (top), and the 3D-printed miniature soft pneumatic robots with high-resolution (bottom). Reproduced with permission.[164] Copyright 2019, Wiley-VCH. b) The powerful optical and sonic transparent hydrogel actuators and their ability to camouflage. Reproduced under the terms of the CC-BY Creative Commons Attribution 4.0 International License.[234d] Copyright 2017, The Authors. Springer Nature. c) Material design, SLA printing system, and the porous actuator (left), and its cooling ability during grasping objects with different heat capacities. Reproduced with permission.[240a] Copyright 2020, AAAS.

environmentally friendly, and stability in extreme environments (for example, extreme temperature). Liquid such as mineral oils or silicone oils, carbon grease, water, and electrorheological fluids can be used according to different needs, such as for cooling and actuation.[240]

Yuk et al. introduced a biomimetic hydrogel-based actuator shown in Figure 12b that can perform hydraulic actuations with high-speed, high-force, and optically and sonically camouflaged in water.[234d] Various applications such as swimming, kicking a ball, or even catching a live goldfish were achieved by the actuator (Figure 12b). Mishra et al. demonstrated a soft hydraulic "smart" hand that can regulate its temperature by autonomic, localized sweating through microscale pores.[240a] As shown in Figure 12c, the fingers of the hand were printed with dynamic pores whose size varies with temperature via a custom-built multimaterial SLA system. pNIPAM and PAAm were selected to make up the body and fingers of the actuator respectively. Due to the distinct responses to temperature of these two composites, the PAAm layer expands under high temperature ($T > 30$ °C), causing the pores to increase their diameter, resulting in the pressurizing fluid "sweating" out of

the actuator. The grasping and object cooling test show the conformability and cooling ability of the gripper to hold different objects with different heat capacity, as shown in Figure 12c.

In addition to hydrogel-based actuators, Hsu et al. demonstrated a DLP 3D printing strategy that can make photoactive elastomer resin-based soft actuators with embedded power sources.[241] Specifically, osmosis, as the driving force, is generated by a flexible composite structure with a semipermeable interface, and the actuator performs elongation, contraction, bending, and torsion under the drive of internal and external osmotic pressure. An osmotic orthodontic actuator and an asymmetric bellow actuator were fabricated, respectively. In addition, Cavaiani et al. designed and fabricated a multiscale capillary gripper via combining SLA and TPP printing technologies that can pick and place sub-millimetric 1005 SMD components.[242] The high precision and ability to print fine structures of the TPP enables the printed picking head picking, aligning, releasing and picking off the micrometer-scale component, and the similarity of the resins used in the two techniques provide a good adherence between parts.

Although the traditional strategies for fabricating pneumatic and hydraulic actuators are still preferred by commercial

large-scale manufacturing, VP may realize manufacturing in one single step and print structure of tiny features with functions of camouflage, "perspiration" and self-healing.[243] In addition, along with the development of higher efficiency and higher resolution VP system, multimaterial soft pneumatic robots at millimeter scale with micrometer features, enhanced performance and functionality will be able to be printed in the future.

5. Conclusions and Future Prospects

Soft electronics is a hotspot undergoing fascinating research currently mainly due to their 1) conformally adhered specialty to irregularly shaped surfaces; 2) intrinsic flexible tactile sensing capability; 3) secure human–machine interface. As the core components of soft electronics, the research of soft sensors and actuators involves multidisciplinary sciences, including physics and biochemistry principles, advanced materials science, optic and electronic technologies, message communication, and artificial intelligence, and presents exuberant vitality in the recent decades.

We have overviewed the recent progress in VP 3D printing technologies for the soft electronic devices' fabrication. Benefiting from the digital computer-assisted design, the AM is capable of providing a versatile platform for patterning of advanced functional materials and complex multicomponent architectures to achieve accelerated transfer from ideas to devices and customized manufacturing. These fabrication systems, accompanied by polymer materials with intrinsic stretchability, biocompatibility, and self-healing ability conform with the development trends of soft sensor and actuator devices. If developed fully, the wearable soft electronic system can enable wearable health monitoring, diagnostics, and continuous treatment. Also, smart sensor and actuator conjugation will endow robotics and prosthetics with a "sense of touch", and environmental perception enabling a variety of currently impossible tasks, such as compliant manipulation of various objects and interaction with humans. Beneath this mission and vision, however, there remain many challenges, which we summarize succinctly as follows:

1) Manufacturing efficiency and structural integrality: one important objective of VP 3D printing is to print objects with complex shapes, compositions, gradients, and functions in a single step, unparalleled by formative and subtractive polymer processing. However, most 3D printing technologies are essentially repeating 2D printing processes over and over again (so-called layer-by-layer), both the build speed and performance of the resulting objects are inferior to those of formative processing like injection molding.[13] The ongoing transition from concept modeling to rapid manufacturing has required significant improvements of cycle times together with crosslinked properties and durability. Furthermore, eliminating the need for support layer and post-treatment steps is essential for improving the competitiveness of VP 3D printing.

2) Insufficiency of the accessible material system: advanced materials are at the heart of future soft electronics. One of the greatest challenges in VP 3D printing to fabricate sensors and actuators is the limitation in available functional materials compared to structural materials. For example, high conductive polymer materials used to produce electrodes are still quite limited compared to conventional metal materials, resulting in a severe connection to the external system due to the modulus mismatch. However, most of the already attempted materials in 3D printing area are not optimized yet for the process due to several practical reasons such as the lack of thorough understanding of each process and its material property requirements. The application of free-standing, biodegradable, and self-healing materials to devices is still at a proofofconcept stage.

3) Development of multicomponent devices: while current multicomponent devices normally require many separate and fundamentally different processing steps, VP 3D printing holds great promise for simplifying workflow and combining processes into a single 3D print job. It can assemble and integrate the sensitive materials into the functional parts, linking the chip to constitute a self-contained sensor and actuator system. However, the bulky equipment, complex operating system, and extravagant price stifling and diminish its popularity.

4) Application of biological electronics: the specialty VP 3D printing to produce multifunctional objects and systems coincides with the development trend of the customized implants that are biologically active or mimic biological functions by responding with property changes to external stimuli in the future. The technology with natural and synthetic hydrogels as biological matrix coupled with 3D cell culture within these meshes allows for the construction of patient-specific tissues for implantation. Moreover, AM-fabricated 3D cell cultures are being used for drug discovery and rapid biological evaluation of substances without requiring animal testing. Compared with DIW 3D printing, however, it is inevitable that ultraviolet crosslinking affects cells and tissues.

Apart from these challenges, some other problems should be resolved for the practical use of soft electronics fabricated by VP 3D printing as well. For example, devices intended for soft robotics applications should have reasonable composite performance and robustness while being aesthetically suitable. And on this basis, the feasibility of boosting the speed, adhesion, and kinematics of soft actuators should be explored. Devices intended for use in wearable and implantable devices should be user customizable to satisfy the personalized needs of people. In an accident-prone and aging society, VP 3D-printed tissue grafts and customized drug delivery systems offer great hope. However, the use of photocurable polymers has often meant a lack of long-term mechanical robustness and durability. The employed materials should not cause any discomfort or have any negative effect on human skin when attached. They should be easy to remove and provide associated portable power and reliable data during extreme activities. Overall, VP 3D printing is expected to be a disruptive innovation that changes the way we think about fabricating and integrating soft electronic devices distinct from that made by traditional fabrication.

[1] M. Kaur, A. Srivastava, *J. Macromol. Sci., Polym. Rev.* **2002**, *42*, 481.

[2] M. Layani, X. Wang, S. Magdassi, *Adv. Mater.* **2018**, *30*, 1706344.

[3] Z. Zhao, J. Wu, X. Mu, H. Chen, H. J. Qi, D. Fang, *Sci. Adv.* **2017**, *3*, e1602326.

[4] a) M. P. De Beer, H. L. Van Der Laan, M. A. Cole, R. J. Whelan, M. A. Burns, T. F. Scott, *Sci. Adv.* **2019**, *5*, eaau8723; b) J. Schwartz, A. J. Boydston, *Nat. Commun.* **2019**, *10*, 791.

[5] a) X. Ma, X. Qu, W. Zhu, Y.-S. Li, S. Yuan, H. Zhang, J. Liu, P. Wang, C. S. E. Lai, F. Zanella, *Proc. Natl. Acad. Sci. USA* **2016**, *113*, 2206; b) A. K. Miri, D. Nieto, L. Iglesias, H. Goodarzi Hosseinabadi, S. Maharjan, G. U. Ruiz-Esparza, P. Khoshakhlagh, A. Manbachi, M. R. Dokmeci, S. Chen, *Adv. Mater.* **2018**, *30*, 1800242.

[6] J. Z. Gul, M. Sajid, M. M. Rehman, G. U. Siddiqui, I. Shah, K.-H. Kim, J.-W. Lee, K. H. Choi, *Sci. Technol. Adv. Mater.* **2018**, *19*, 243.

[7] J. C. Yeo, H. K. Yap, W. Xi, Z. Wang, C. H. Yeow, C. T. Lim, *Adv. Mater. Technol.* **2016**, *1*, 1600018.

[8] Y. Ling, T. An, L. W. Yap, B. Zhu, S. Gong, W. Cheng, *Adv. Mater.* **2020**, *32*, 1904664.

[9] J. C. Yang, J. Mun, S. Y. Kwon, S. Park, Z. Bao, S. Park, *Adv. Mater.* **2019**, *31*, 1904765.

[10] C. G. Núñez, L. Manjakkal, R. Dahiya, *npj Flexible Electron.* **2019**, *3*, 1.

[11] a) Y. Wu, Y. Liu, Y. Zhou, Q. Man, C. Hu, W. Asghar, F. Li, Z. Yu, J. Shang, G. Liu, *Sci. Rob.* **2018**, *3*, eaat0429; b) Z. Zheng, N. Ding, in *2019 IEEE Int. Conf. on Robotics and Automation(ICRA)*, IEEE, **2019**, https://doi.org/10.1109/ICRA.2019.8793562.

[12] a) T. Wallin, J. Pikul, R. Shepherd, *Nat. Rev. Mater.* **2018**, *3*, 84; b) M. T. Tolley, R. F. Shepherd, B. Mosadegh, K. C. Galloway, M. Wehner, M. Karpelson, R. J. Wood, G. M. Whitesides, *Soft Rob.* **2014**, *1*, 213.

[13] L. Y. Zhou, J. Fu, Y. He, *Adv. Funct. Mater.* **2020**, *30*, 2000187.

[14] X. Li, W. Shan, Y. Yang, D. Joralmon, Y. Zhu, Y. Chen, Y. Yuan, H. Xu, J. Rong, R. Dai, *Adv. Funct. Mater.* **2021**, *31*, 2003725.

[15] a) M. N. I. Shiblee, K. Ahmed, A. Khosla, M. Kawakami, H. Furukawa, *Soft Matter* **2018**, *14*, 7809; b) L. Huang, R. Jiang, J. Wu, J. Song, H. Bai, B. Li, Q. Zhao, T. Xie, *Adv. Mater.* **2017**,

[16] C. W. Hull, *U.S. Patent 4575330*, **1986**.

[17] J. del Barrio, C. Sánchez-Somolinos, *Adv. Opt. Mater.* **2019**, *7*, 1900598.

[18] M. D'Angelo, M. V. Chekhova, Y. Shih, *Phys. Rev. Lett.* **2001**, *87*, 013602.

[19] Q. Ge, Z. Li, Z. Wang, W. Zhang, X. He, J. Zhou, N. Fang, *Int. J. Extreme Manuf.* **2020**, *2*, 022004.

[20] *Multiphoton Lithography: Techniques, Materials and Applications* (Eds: J. Stampfl, R. Liska, A. Ovsianikov), Wiley-VCH, Weinheim, Germany **2017**.

[21] G. A. Appuhamillage, N. Chartrain, V. Meenakshisundaram, K. D. Feller, C. B. Williams, T. E. Long, *Ind. Eng. Chem. Res.* **2019**, *58*, 15109.

[22] C. Sun, N. Fang, D. Wu, X. Zhang, *Sens. Actuators, A* **2005**, *121*, 113.

[23] J. R. Tumbleston, D. Shirvanyants, N. Ermoshkin, R. Janusziewicz, A. R. Johnson, D. Kelly, K. Chen, R. Pinschmidt, J. P. Rolland, A. Ermoshkin, *Science* **2015**, *347*, 1349.

[24] S. C. Ligon, R. Liska, J. Stampfl, M. Gurr, R. Mülhaupt, *Chem. Rev.* **2017**, *117*, 10212.

[25] a) M. Vatani, Y. Lu, E. D. Engeberg, J.-W. Choi, *Int. J. Precis. Eng. Manuf.* **2015**, *16*, 1375; b) H. Jeong, Y. Cui, M. M. Tentzeris, S. Lim, *Addit. Manuf.* **2020**, *35*, 101405.

[26] A. T. Gaynor, N. A. Meisel, C. B. Williams, J. K. Guest, *J. Manuf. Sci. Eng.* **2014**, *136*, 061015.

[27] a) S. Sundaram, Z. Jiang, P. Sitthi-Amorn, D. S. Kim, M. A. Baldo, W. Matusik, *Adv. Mater. Technol.* **2017**, *2*, 1600257; b) J. Wu, C. Yuan, Z. Ding, M. Isakov, Y. Mao, T. Wang, M. L. Dunn, H. J. Qi, *Sci. Rep.* **2016**, *6*, 24224.

[28] *Position Sensors* (Ed: D. S. Nyce), Wiley-VCH, Weinheim, Germany **2016**.

[29] G. Gonzalez, A. Chiappone, K. Dietliker, C. F. Pirri, I. Roppolo, *Adv. Mater. Technol.* **2020**, *5*, 2000374.

[30] C. Yang, Z. Suo, *Nat. Rev. Mater.* **2018**, *3*, 125.

[31] Z. Wang, Y. Cong, J. Fu, *J. Mater. Chem. B* **2020**, *8*, 3437.

[32] a) Y. Song, H. Chen, Z. Su, X. Chen, L. Miao, J. Zhang, X. Cheng, H. Zhang, *Small* **2017**, *13*, 1702091; b) J. Pignanelli, K. Schlingman, T. B. Carmichael, S. Rondeau-Gagné, M. J. Ahamed, *Sens. Actuators, A* **2019**, *285*, 427.

[33] H. B. Yao, J. Ge, C. F. Wang, X. Wang, W. Hu, Z. J. Zheng, Y. Ni, S. H. Yu, *Adv. Mater.* **2013**, *25*, 6692.

[34] M.-j. Yin, Y. Zhang, Z. Yin, Q. Zheng, A. P. Zhang, *Adv. Mater. Technol.* **2018**, *3*, 1800051.

[35] I. J. Kim, J. E. Lee, J. W. Ko, J. Jung, A. S. Lee, D. J. Lee, S. G. Lee, B.-I. Park, S. Yu, J. H. Lee, *Mater. Lett.* **2020**, *268*, 127565.

[36] Q. Zhang, Y. L. Wang, Y. Xia, P. F. Zhang, T. V. Kirk, X. D. Chen, *Adv. Mater. Technol.* **2019**, *4*, 1900485.

[37] a) S. J. Park, J. Kim, M. Chu, M. Khine, *Adv. Mater. Technol.* **2018**, *3*, 1700158; b) R. Ramalingame, A. Lakshmanan, F. Müller, U. Thomas, O. Kanoun, *J. Sens. Sens. Syst.* **2019**, *8*, 87.

[38] L.-Q. Tao, K.-N. Zhang, H. Tian, Y. Liu, D.-Y. Wang, Y.-Q. Chen, Y. Yang, T.-L. Ren, *ACS Nano* **2017**, *11*, 8790.

[39] a) N. Luo, W. Dai, C. Li, Z. Zhou, L. Lu, C. C. Poon, S. C. Chen, Y. Zhang, N. Zhao, *Adv. Funct. Mater.* **2016**, *26*, 1178; b) T. D. Gupta, T. Gacoin, A. Rowe, *Adv. Funct. Mater.* **2014**, *24*, 4522; c) T. Y. Choi, B.-U. Hwang, B.-Y. Kim, T. Q. Trung, Y. H. Nam, D.-N. Kim, K. Eom, N.-E. Lee, *ACS Appl. Mater. Interfaces* **2017**, *9*, 18022; d) D. H. Ho, R. Song, Q. Sun, W.-H. Park, S. Y. Kim, C. Pang, D. H. Kim, S.-Y. Kim, J. Lee, J. H. Cho, *ACS Appl. Mater. Interfaces* **2017**, *9*, 44678.

[40] T. Wang, Y. Zhang, Q. Liu, W. Cheng, X. Wang, L. Pan, B. Xu, H. Xu, *Adv. Funct. Mater.* **2018**, *28*, 1705551.

[41] J. Oh, J. O. Kim, Y. Kim, H. B. Choi, J. C. Yang, S. Lee, M. Pyatykh, J. Kim, J. Y. Sim, S. Park, *Small* **2019**, *15*, 1901744.

[42] Z. Wang, S. Wang, J. Zeng, X. Ren, A. J. Chee, B. Y. Yiu, W. C. Chung, Y. Yang, A. C. Yu, R. C. Roberts, *Small* **2016**, *12*, 3827.

[43] A. D. Valentine, T. A. Busbee, J. W. Boley, J. R. Raney, A. Chortos, A. Kotikian, J. D. Berrigan, M. F. Durstock, J. A. Lewis, *Adv. Mater.* **2017**, *29*, 1703817.

[44] W. Li, L. S. Mille, J. A. Robledo, T. Uribe, V. Huerta, Y. S. Zhang, *Adv. Healthcare Mater.* **2020**, *9*, 2000156.

[45] Y. Zhang, F. Zhang, Z. Yan, Q. Ma, X. Li, Y. Huang, J. A. Rogers, *Nat. Rev. Mater.* **2017**, *2*, 17019.

[46] E. Fantino, A. Chiappone, I. Roppolo, D. Manfredi, R. Bongiovanni, C. F. Pirri, F. Calignano, *Adv. Mater.* **2016**, *28*, 3712.

[47] Y. Shao, Y. Zhao, M. Liu, Q. Zhang, C. Liu, in *2018 IEEE Sensors*, IEEE, **2018**, https://doi.org/10.1109/ICSENS.2018.8589555.

[48] S. Peng, Y. Li, L. Wu, J. Zhong, Z. Weng, L. Zheng, Z. Yang, J.-T. Miao, *ACS Appl. Mater. Interfaces* **2020**, *12*, 6479.

[49] T. Zhao, R. Yu, S. Li, X. Li, Y. Zhang, X. Yang, X. Zhao, C. Wang, Z. Liu, R. Dou, W. Huang, *ACS Appl. Mater. Interfaces* **2019**, *11*, 14391.

[50] D. K. Patel, A. H. Sakhaei, M. Layani, B. Zhang, Q. Ge, S. Magdassi, *Adv. Mater.* **2017**, *29*, 1606000.

[51] K. Yu, A. Xin, H. Du, Y. Li, Q. Wang, *NPG Asia Mater.* **2019**, *11*, 7.

[52] Y. Yang, X. Li, M. Chu, H. Sun, J. Jin, K. Yu, Q. Wang, Q. Zhou, Y. Chen, *Sci. Adv.* **2019**, *5*, eaau9490.

[53] Q. Mu, L. Wang, C. K. Dunn, X. Kuang, F. Duan, Z. Zhang, H. J. Qi, T. Wang, *Addit. Manuf.* **2017**, *18*, 74.

[54] X.-Y. Yin, Y. Zhang, X. Cai, Q. Guo, J. Yang, Z. L. Wang, *Mater. Horiz.* **2019**, *6*, 767.

[55] X. Y. Yin, Y. Zhang, J. Xiao, C. Moorlag, J. Yang, *Adv. Funct. Mater.* **2019**, *29*, 1904716.

[56] K. Kim, W. Zhu, X. Qu, C. Aaronson, W. R. McCall, S. Chen, D. J. Sirbuly, *ACS Nano* **2014**, *8*, 9799.

[57] a) H. Cui, R. Hensleigh, D. Yao, D. Maurya, P. Kumar, M. G. Kang, S. Priya, X. R. Zheng, *Nat. Mater.* **2019**, *18*, 234; b) D. Yao, H. Cui, R. Hensleigh, P. Smith, S. Alford, D. Bernero, S. Bush, K. Mann, H. F. Wu, M. Chin-Nieh, *Adv. Funct. Mater.* **2019**, *29*, 1903866.

[58] J. Zhang, S. Ye, H. Liu, X. Chen, X. Chen, B. Li, W. Tang, Q. Meng, P. Ding, H. Tian, *Nano Energy* **2020**, *77*, 105300.

[59] X. Chen, H. O. T. Ware, E. Baker, W. Chu, J. Hu, C. Sun, *Proc. CIRP* **2017**, *65*, 157.

[60] Y. Huang, X. Fan, S. C. Chen, N. Zhao, *Adv. Funct. Mater.* **2019**, *29*, 1808509.

[61] a) M. Liu, Q. Zhang, Y. Shao, C. Liu, Y. Zhao, *Micromachines* **2018**, *10*, 20; b) J. Qu, Q. Wu, T. Clancy, Q. Fan, X. Wang, X. Liu, *IEEE Sens. J.* **2020**, *20*, 6971; c) F. Lucklum, G. Dumstorff, in *2016 IEEE Sensors*, IEEE, **2016**, https://doi.org/10.1109/ICSENS.2016.7808633; d) J. H. Kang, J. Y. Kim, Y. Jo, H.-S. Kim, S. M. Jung, S. Y. Lee, Y. Choi, S. Jeong, *RSC Adv.* **2019**, *9*, 39993; e) C. Didier, A. Kundu, S. Rajaraman, *Microsyst. Nanoeng.* **2020**, *6*, 15.

[62] Y. Zhou, Y. Wu, W. Asghar, J. Ding, X. Su, S. Li, F. Li, Z. Yu, J. Shang, Y. Liu, R.-W. Li, *ACS Appl. Electron. Mater.* **2019**, *1*, 1866.

[63] R. Hagihghi, A. Razmjou, Y. Orooji, M. E. Warkiani, M. Asadnia, *J. Biomed. Mater. Res., Part B* **2020**, *108*, 568.

[64] L. J. Tan, W. Zhu, K. Zhou, *Adv. Funct. Mater.* **2020**, *30*, 2003062.

[65] X. Wang, Q. Guo, X. Cai, S. Zhou, B. Kobe, J. Yang, *ACS Appl. Mater. Interfaces* **2014**, *6*, 2583.

[66] M. Nadgorny, A. Ameli, *ACS Appl. Mater. Interfaces* **2018**, *10*, 17489.

[67] A. Sakly, S. Kenzari, D. Bonina, S. Corbel, V. Fournée, *Mater. Des.* **2014**, *56*, 280.

[68] a) C. Lu, C. Wang, J. Yu, J. Wang, F. Chu, *ChemSusChem* **2020**, *13*, 893; b) R. Hensleigh, H. Cui, Z. Xu, J. Massman, D. Yao, J. Berrigan, X. Zheng, *Nat. Electron.* **2020**, *3*, 216.

[69] S. Li, H. Bai, R. F. Shepherd, H. Zhao, *Angew. Chem., Int. Ed.* **2019**, *58*, 11182.

[70] M. Invernizzi, S. Turri, M. Levi, R. Suriano, *Eur. Polym. J.* **2018**, *101*, 169.

[71] W. A. D. M. Jayathilaka, K. Qi, Y. Qin, A. Chinnappan, W. Serrano-García, C. Baskar, H. Wang, J. He, S. Cui, S. W. Thomas, *Adv. Mater.* **2019**, *31*, 1805921.

[72] S. Kang, J. Lee, S. Lee, S. Kim, J. K. Kim, H. Algadi, S. Al-Sayari, D. E. Kim, D. Kim, T. Lee, *Adv. Electron. Mater.* **2016**, *2*, 1600356.

[73] F. Xu, Y. Zhu, *Adv. Mater.* **2012**, *24*, 5117.

[74] T. Yang, D. Xie, Z. Li, H. Zhu, *Mater. Sci. Eng., R* **2017**, *115*, 1.

[75] a) Q. Su, Q. Huang, K. Lan, T. Xue, W. Gao, Q. Zou, *J. Micromech. Microeng.* **2019**, *30*, 015009; b) S. R. A. Ruth, L. Beker, H. Tran, V. R. Feig, N. Matsuhisa, Z. Bao, *Adv. Funct. Mater.* **2019**, *30*, 1903100.

[76] K. Xu, Y. Lu, K. Takei, *Adv. Mater. Technol.* **2019**, *4*, 1800628.

[77] W. Yang, N. W. Li, S. Zhao, Z. Yuan, J. Wang, X. Du, B. Wang, R. Cao, X. Li, W. Xu, *Adv. Mater. Technol.* **2018**, *3*, 1700241.

[78] Y. Xiong, Y. Shen, L. Tian, Y. Hu, P. Zhu, R. Sun, C.-P. Wong, *Nano Energy* **2020**, *70*, 104436.

[79] S. C. Mannsfeld, B. C. Tee, R. M. Stoltenberg, C. V. H. Chen, S. Barman, B. V. Muir, A. N. Sokolov, C. Reese, Z. Bao, *Nat. Mater.* **2010**, *9*, 859.

[80] H. Kim, G. Kim, T. Kim, S. Lee, D. Kang, M. S. Hwang, Y. Chae, S. Kang, H. Lee, H. G. Park, *Small* **2018**, *14*, 1703432.

[81] B. Nie, R. Li, J. Cao, J. D. Brandt, T. Pan, *Adv. Mater.* **2015**, *27*, 6055.

[82] F. Li, D. Lin, Z. Chen, Z. Cheng, J. Wang, C. Li, Z. Xu, Q. Huang, X. Liao, L.-Q. Chen, *Nat. Mater.* **2018**, *17*, 349.

[83] D. Y. Park, D. J. Joe, D. H. Kim, H. Park, J. H. Han, C. K. Jeong, H. Park, J. G. Park, B. Joung, K. J. Lee, *Adv. Mater.* **2017**, *29*, 1702308.

[84] L. Natta, V. Mastronardi, F. Guido, L. Algieri, S. Puce, F. Pisano, F. Rizzi, R. Pulli, A. Qualtieri, M. De Vittorio, *Sci. Rep.* **2019**, *9*, 8392.

[85] W. Deng, T. Yang, L. Jin, C. Yan, H. Huang, X. Chu, Z. Wang, D. Xiong, G. Tian, Y. Gao, *Nano Energy* **2019**, *55*, 516.

[86] Z. Chen, Z. Wang, X. Li, Y. Lin, N. Luo, M. Long, N. Zhao, J.-B. Xu, *ACS Nano* **2017**, *11*, 4507.

[87] Y. Yang, H. Pan, G. Xie, Y. Jiang, C. Chen, Y. Su, Y. Wang, H. Tai, *Sens. Actuators, A* **2020**, *301*, 111789.

[88] D. P. Lannes, A. L. Gama, T. F. B. Bento, *Flow Meas. Instrum.* **2018**, *60*, 208.

[89] T. Huang, S. Yang, P. He, J. Sun, S. Zhang, D. Li, Y. Meng, J. Zhou, H. Tang, J. Liang, *ACS Appl. Mater. Interfaces* **2018**, *10*, 30732.

[90] X. Chen, X. Li, J. Shao, N. An, H. Tian, C. Wang, T. Han, L. Wang, B. Lu, *Small* **2017**, *13*, 1604245.

[91] K. S. Ramadan, D. Sameoto, S. Evoy, *Smart Mater. Struct.* **2014**, *23*, 033001.

[92] a) J. Z. Manapat, Q. Chen, P. Ye, R. C. Advincula, *Macromol. Mater. Eng.* **2017**, *302*, 1600553; b) E. Zanchetta, M. Cattaldo, G. Franchin, M. Schwentenwein, J. Homa, G. Brusatin, P. Colombo, *Adv. Mater.* **2016**, *28*, 370.

[93] K. I. Park, M. Lee, Y. Liu, S. Moon, G. T. Hwang, G. Zhu, J. E. Kim, S. O. Kim, D. K. Kim, Z. L. Wang, *Adv. Mater.* **2012**, *24*, 2999.

[94] H. Kim, L. C. D. Manriquez, M. T. Islam, L. A. Chavez, J. E. Regis, M. A. Ahsan, J. C. Noveron, T.-L. B. Tseng, Y. Lin, *MRS Commun.* **2019**, *9*, 1115.

[95] J. Cha, J. W. Lee, B. Bae, S.-E. Lee, C.-B. Yoon, *J. Korean Ceram. Soc.* **2019**, *56*, 360.

[96] W. Wang, J. Sun, B. Guo, X. Chen, K. P. Ananth, J. Bai, *J. Eur. Ceram. Soc.* **2020**, *40*, 682.

[97] C. Dagdeviren, Y. Su, P. Joe, R. Yona, Y. Liu, Y.-S. Kim, Y. Huang, A. R. Damadoran, J. Xia, L. W. Martin, *Nat. Commun.* **2014**, *5*, 4496.

[98] S. Guerin, S. A. Tofail, D. Thompson, *NPG Asia Mater.* **2019**, *11*, 10.

[99] L. Persano, C. Dagdeviren, Y. Su, Y. Zhang, S. Girardo, D. Pisignano, Y. Huang, J. A. Rogers, *Nat. Commun.* **2013**, *4*, 1633.

[100] B. Tiller, A. Reid, B. Zhu, J. Guerreiro, R. Domingo-Roca, J. C. Jackson, J. Windmill, *Mater. Des.* **2019**, *165*, 107593.

[101] Z. Chen, X. Song, L. Lei, X. Chen, C. Fei, C. T. Chiu, X. Qian, T. Ma, Y. Yang, K. Shung, *Nano Energy* **2016**, *27*, 78.

**ADVANCED
SCIENCE NEWS**

www.advancedsciencenews.com

**ADVANCED
MATERIALS
TECHNOLOGIES**

www.advmattechnol.de

[102] S. Laurent, D. Forge, M. Port, A. Roch, C. Robic, L. Vander Elst, R. N. Muller, *Chem. Rev.* **2008**, *108*, 2064.

[103] S. Lantean, G. Barrera, C. F. Pirri, P. Tiberto, M. Sangermano, I. Roppolo, G. Rizza, *Adv. Mater. Technol.* **2019**, *4*, 1900505.

[104] Z. Ji, C. Yan, B. Yu, X. Wang, F. Zhou, *Adv. Mater. Interfaces* **2017**, *4*, 1700629.

[105] C. Credi, A. Fiorese, M. Tironi, R. Bernasconi, L. Magagnin, M. Levi, S. Turri, *ACS Appl. Mater. Interfaces* **2016**, *8*, 26332.

[106] O. S. Wenger, *Chem. Rev.* **2013**, *113*, 3686.

[107] N. Maldonado, V. G. Vegas, O. Halevi, J. I. Martínez, P. S. Lee, S. Magdassi, M. T. Wharmby, A. E. Platero-Prats, C. Moreno, F. Zamora, *Adv. Funct. Mater.* **2019**, *29*, 1808424.

[108] H. Zhu, H. Yang, Y. Ma, T. J. Lu, F. Xu, G. M. Genin, M. Lin, *Adv. Funct. Mater.* **2020**, *30*, 2000639.

[109] K. Kabiri, H. Omidian, M. Zohuriaan-Mehr, S. Doroudiani, *Polym. Compos.* **2011**, *32*, 277.

[110] M. J. Yin, M. Yao, S. Gao, A. P. Zhang, H. Y. Tam, P. K. A. Wai, *Adv. Mater.* **2016**, *28*, 1394.

[111] X. Li, Y. Yang, B. Xie, M. Chu, H. Sun, S. Hao, Y. Chen, Y. Chen, *Adv. Mater. Technol.* **2019**, *4*, 1800476.

[112] L. Y. Yeo, H. C. Chang, P. P. Chan, J. R. Friend, *Small* **2011**, *7*, 12.

[113] R. Dong, Y. Liu, L. Mou, J. Deng, X. Jiang, *Adv. Mater.* **2019**, *31*, 1805033.

[114] J. C. McDonald, G. M. Whitesides, *Acc. Chem. Res.* **2002**, *35*, 491.

[115] Y. He, J.-Z. Fu, Z.-C. Chen, *J. Micromech. Microeng.* **2007**, *17*, 2420.

[116] U. M. Attia, S. Marson, J. R. Alcock, *Microfluid. Nanofluid.* **2009**, *7*, 1.

[117] X. Ruan, Y. Wang, N. Cheng, X. Niu, Y. C. Chang, L. Li, D. Du, Y. Lin, *Adv. Mater. Technol.* **2020**, *5*, 2000171.

[118] A. Lambert, S. Valiulis, Q. Cheng, *ACS Sens.* **2018**, *3*, 2475.

[119] A. K. Au, W. Lee, A. Folch, *Lab Chip* **2014**, *14*, 1294.

[120] a) L. Cevenini, M. M. Calabretta, G. Tarantino, E. Michelini, A. Roda, *Sens. Actuators, B* **2016**, *225*, 249; b) A. Roda, M. Guardigli, D. Calabria, M. M. Calabretta, L. Cevenini, E. Michelini, *Analyst* **2014**, *139*, 6494; c) Y. Wang, M. M. Zeinhom, M. Yang, R. Sun, S. Wang, J. N. Smith, C. Timchalk, L. Li, Y. Lin, D. Du, *Anal. Chem.* **2017**, *89*, 9339.

[121] A. P. Kuo, N. Bhattacharjee, Y. S. Lee, K. Castro, Y. T. Kim, A. Folch, *Adv. Mater. Technol.* **2019**, *4*, 1800395.

[122] a) M. J. Männel, L. Selzer, R. Bernhardt, J. Thiele, *Adv. Mater. Technol.* **2019**, *4*, 1800408; b) C. Barner-Kowollik, M. Bastmeyer, E. Blasco, G. Delaittre, P. Müller, B. Richter, M. Wegener, *Angew. Chem., Int. Ed.* **2017**, *56*, 15828.

[123] a) C. Schizas, V. Melissinaki, A. Gaidukeviciute, C. Reinhardt, C. Ohrt, V. Dedoussis, B. N. Chichkov, C. Fotakis, M. Farsari, D. Karalekas, *Int. J. Adv. Manuf. Technol.* **2010**, *48*, 435; b) A. K. Au, N. Bhattacharjee, L. F. Horowitz, T. C. Chang, A. Folch, *Lab Chip* **2015**, *15*, 1934.

[124] Z. F. Rad, R. E. Nordon, C. J. Anthony, L. Bilston, P. D. Prewett, J.-Y. Arns, C. H. Arns, L. Zhang, G. J. Davies, *Microsyst. Nanoeng.* **2017**, *3*, 17034.

[125] T. Ching, Y.-C. Toh, M. Hashimoto, *Adv. Eng. Mater.* **2020**, *22*, 1901109.

[126] S. Zips, O. J. Wenzel, P. Rinklin, L. Grob, K. Terkan, N. Y. Adly, L. Weiß, B. Wolfrum, *Adv. Mater. Technol.* **2019**, *4*, 1800455.

[127] a) T. Kamperman, L. M. Teixeira, S. S. Salehi, G. Kerckhofs, Y. Guyot, M. Geven, L. Geris, D. Grijpma, S. Blanquer, J. Leijten, *Lab Chip* **2020**, *20*, 490; b) D. H. Kang, N. K. Kim, S. W. Park, W. Lee, H. W. Kang, *Lab Chip* **2020**, *20*, 4433.

[128] G. Weisgrab, A. Ovsianikov, P. F. Costa, *Adv. Mater. Technol.* **2019**, *4*, 1900275.

[129] J. Y. Han, B. Krasniqi, J. Kim, M. Keckley, D. L. DeVoe, *Adv. Mater. Technol.* **2020**, *5*, 1901105.

[130] S. Hampson, W. Rowe, S. D. Christie, M. Platt, *Sens. Actuators, B* **2018**, *256*, 1030.

[131] Y. He, Y. Wu, J. z. Fu, Q. Gao, J. j. Qiu, *Electroanalysis* **2016**, *28*, 1658.

[132] a) Z. Cai, N. L. Smith, J.-T. Zhang, S. A. Asher, *Anal. Chem.* **2015**, *87*, 5013; b) M. R. Khosravani, T. Reinicke, *Sens. Actuators, A* **2020**, *305*, 111916.

[133] G. W. Bishop, J. E. Satterwhite-Warden, I. Bist, E. Chen, J. F. Rusling, *ACS Sens.* **2016**, *1*, 197.

[134] C. Tang, A. Vaze, J. Rusling, *Lab Chip* **2017**, *17*, 484.

[135] K. Kadimisetty, S. Malla, J. F. Rusling, *ACS Sens.* **2017**, *2*, 670.

[136] K. Kadimisetty, S. Malla, K. S. Bhalerao, I. M. Mosa, S. Bhakta, N. H. Lee, J. F. Rusling, *Anal. Chem.* **2018**, *90*, 7569.

[137] A. M. Nightingale, C. L. Leong, R. A. Burnish, S.-u. Hassan, Y. Zhang, G. F. Clough, M. G. Boutelle, D. Voegeli, X. Niu, *Nat. Commun.* **2019**, *10*, 2741.

[138] a) H. N. Chan, Y. Chen, Y. Shu, Y. Chen, Q. Tian, H. Wu, *Microfluid. Nanofluid.* **2015**, *19*, 9; b) N. Bhattacharjee, C. Parra-Cabrera, Y. T. Kim, A. P. Kuo, A. Folch, *Adv. Mater.* **2018**, *30*, 1800001.

[139] A. Urrios, C. Parra-Cabrera, N. Bhattacharjee, A. M. Gonzalez-Suarez, L. G. Rigat-Brugarolas, U. Nallapatti, J. Samitier, C. A. DeForest, F. Posas, J. L. Garcia-Cordero, *Lab Chip* **2016**, *16*, 2287.

[140] C. A. Mandon, L. J. Blum, C. A. Marquette, *Anal. Chem.* **2016**, *88*, 10767.

[141] A. Chiadò, G. Palmara, A. Chiappone, C. Tanzanu, C. F. Pirri, I. Roppolo, F. Frascella, *Lab Chip* **2020**, *20*, 665.

[142] R. M. Dirkzwager, S. Liang, J. A. Tanner, *ACS Sens.* **2016**, *1*, 420.

[143] M. J. Beauchamp, A. V. Nielsen, H. Gong, G. P. Nordin, A. T. Woolley, *Anal. Chem.* **2019**, *91*, 7418.

[144] V. Bertana, G. Scordo, M. Parmeggiani, L. Scaltrito, S. Ferrero, M. G. Gomez, M. Cocuzza, D. Vurro, P. D'Angelo, S. Iannotta, *Sci. Rep.* **2020**, *10*, 13335.

[145] A. D. Tadmor, E. A. Ottesen, J. R. Leadbetter, R. Phillips, *Science* **2011**, *333*, 58.

[146] M. S. Chiriaco, E. Primiceri, E. d'Amone, R. E. Ionescu, R. Rinaldi, G. Maruccio, *Lab Chip* **2011**, *11*, 658.

[147] a) N. Ramanujam, in *Encyclopedia of Analytical Chemistry* (Ed: R. A. Meyers), Wiley-VCH, Weinheim, Germany **2006**; b) A. Tycova, J. Prikryl, F. Foret, *Electrophoresis* **2017**, *38*, 1977.

[148] J. Han, H. Cheng, B. Wang, M. S. Braun, X. Fan, M. Bender, W. Huang, C. Domhan, W. Mier, T. Lindner, *Angew. Chem., Int. Ed.* **2017**, *56*, 15246.

[149] W. Lee, D. Kwon, W. Choi, G. Y. Jung, A. K. Au, A. Folch, S. Jeon, *Sci. Rep.* **2015**, *5*, 7717.

[150] J. Homola, S. S. Yee, G. Gauglitz, *Sens. Actuators, B* **1999**, *54*, 3.

[151] S. S. Hinman, K. S. McKeating, Q. Cheng, *Anal. Chem.* **2017**, *89*, 12626.

[152] J. Arlett, E. Myers, M. Roukes, *Nat. Nanotechnol.* **2011**, *6*, 203.

[153] L. P. C. Gomez, A. Spangenberg, X. A. Ton, Y. Fuchs, F. Bokeloh, J. P. Malval, B. Tse Sum Bui, D. Thuau, C. Ayela, K. Haupt, *Adv. Mater.* **2016**, *28*, 5931.

[154] S. Stassi, E. Fantino, R. Calmo, A. Chiappone, M. Gillono, D. Scaiola, C. F. Pirri, C. Ricciardi, A. Chiadò, I. Roppolo, *ACS Appl. Mater. Interfaces* **2017**, *9*, 19193.

[155] J. M. McCracken, B. R. Donovan, T. J. White, *Adv. Mater.* **2020**, *32*, 1906564.

[156] S. Jiang, F. Liu, A. Lerch, L. Ionov, S. Agarwal, *Adv. Mater.* **2015**, *27*, 4865.

[157] M. Ma, L. Guo, D. G. Anderson, R. Langer, *Science* **2013**, *339*, 186.

[158] a) B. Xue, M. Qin, T. Wang, J. Wu, D. Luo, Q. Jiang, Y. Li, Y. Cao, W. Wang, *Adv. Funct. Mater.* **2016**, *26*, 9053; b) Y. Wang, Q. Guo, G. Su, J. Cao, J. Liu, X. Zhang, *Adv. Funct. Mater.* **2019**, *29*, 1906198.

[159] G. Stoychev, A. Kirillova, L. Ionov, *Adv. Opt. Mater.* **2019**, *7*, 1900067.

[160] B. Mosadegh, P. Polygerinos, C. Keplinger, S. Wennstedt, R. F. Shepherd, U. Gupta, J. Shim, K. Bertoldi, C. J. Walsh, G. M. Whitesides, *Adv. Funct. Mater.* **2014**, *24*, 2163.

[161] L. Hines, K. Petersen, G. Z. Lum, M. Sitti, *Adv. Mater.* **2017**, *29*, 1603483.

**ADVANCED
SCIENCE NEWS**

www.advancedsciencenews.com

**ADVANCED
MATERIALS
TECHNOLOGIES**

www.advmattechnol.de

[162] X. Pang, J.-a. Lv, C. Zhu, L. Qin, Y. Yu, *Adv. Mater.* **2019**, *31*, 1904224.

[163] X. Le, W. Lu, J. Zhang, T. Chen, *Adv. Sci.* **2019**, *6*, 1801584.

[164] Y. F. Zhang, C. J. X. Ng, Z. Chen, W. Zhang, S. Panjwani, K. Kowsari, H. Y. Yang, Q. Ge, *Adv. Mater. Technol.* **2019**, *4*, 1900427.

[165] S. Tibbits, *Archit. Des.* **2014**, *84*, 116.

[166] X. Kuang, D. J. Roach, J. Wu, C. M. Hamel, Z. Ding, T. Wang, M. L. Dunn, H. J. Qi, *Adv. Funct. Mater.* **2019**, *29*, 1805290.

[167] J. M. McCracken, B. M. Rauzan, J. C. Kjellman, H. Su, S. A. Rogers, R. G. Nuzzo, *Adv. Funct. Mater.* **2019**, *29*, 1806723.

[168] D. Han, R. S. Morde, S. Mariani, A. A. La Mattina, E. Vignali, C. Yang, G. Barillaro, H. Lee, *Adv. Funct. Mater.* **2020**, *30*, 1909197.

[169] Z. Zhang, N. Corrigan, A. Bagheri, J. Jin, C. Boyer, *Angew. Chem.* **2019**, *131*, 18122.

[170] H. Wu, X. Zhang, Z. Ma, C. Zhang, J. Ai, P. Chen, C. Yan, B. Su, Y. Shi, *Adv. Sci.* **2020**, *7*, 1903208.

[171] S. Dadbakhsh, M. Speirs, J. P. Kruth, J. Schrooten, J. Luyten, J. Van Humbeeck, *Adv. Eng. Mater.* **2014**, *16*, 1140.

[172] G. Liu, Y. Zhao, G. Wu, J. Lu, *Sci. Adv.* **2018**, *4*, eaat0641.

[173] Q. Ze, X. Kuang, S. Wu, J. Wong, S. M. Montgomery, R. Zhang, J. M. Kovitz, F. Yang, H. J. Qi, R. Zhao, *Adv. Mater.* **2020**, *32*, 1906657.

[174] B. Aksoy, H. Shea, *Adv. Funct. Mater.* **2020**, *30*, 2001597.

[175] E. C. Davidson, A. Kotikian, S. Li, J. Aizenberg, J. A. Lewis, *Adv. Mater.* **2020**, *32*, 1905682.

[176] M. Champeau, D. A. Heinze, T. N. Viana, E. R. de Souza, A. C. Chinellato, S. Titotto, *Adv. Funct. Mater.* **2020**, *30*, 1910606.

[177] J. Leng, X. Lan, Y. Liu, S. Du, *Prog. Mater. Sci.* **2011**, *56*, 1077.

[178] a) M. D. Hager, S. Bode, C. Weber, U. S. Schubert, *Prog. Polym. Sci.* **2015**, *49*, 3; b) K. Yu, Q. Ge, H. J. Qi, *Nat. Commun.* **2014**, *5*, 3066.

[179] a) K. Yu, M. L. Dunn, H. J. Qi, *Extreme Mech. Lett.* **2015**, *4*, 9; b) Z. Ding, C. Yuan, X. Peng, T. Wang, H. J. Qi, M. L. Dunn, *Sci. Adv.* **2017**, *3*, e1602890.

[180] Y. Mao, K. Yu, M. S. Isakov, J. Wu, M. L. Dunn, H. J. Qi, *Sci. Rep.* **2015**, *5*, 13616.

[181] Y. Y. C. Choong, S. Maleksaeedi, H. Eng, J. Wei, P.-C. Su, *Mater. Des.* **2017**, *126*, 219.

[182] S. Joshi, K. Rawat, C. Karunakaran, V. Rajamohan, A. T. Mathew, K. Koziol, V. K. Thakur, A. Balan, *Appl. Mater. Today* **2020**, *18*, 100490.

[183] M. Behl, K. Kratz, U. Noechel, T. Sauter, A. Lendlein, *Proc. Natl. Acad. Sci. USA* **2013**, *110*, 12555.

[184] B. Zhang, W. Zhang, Z. Zhang, Y.-F. Zhang, H. Hingorani, Z. Liu, J. Liu, Q. Ge, *ACS Appl. Mater. Interfaces* **2019**, *11*, 10328.

[185] J.-T. Miao, M. Ge, S. Peng, J. Zhong, Y. Li, Z. Weng, L. Wu, L. Zheng, *ACS Appl. Mater. Interfaces* **2019**, *11*, 40642.

[186] R. Yu, X. Yang, Y. Zhang, X. Zhao, X. Wu, T. Zhao, Y. Zhao, W. Huang, *ACS Appl. Mater. Interfaces* **2017**, *9*, 1820.

[187] Q. Ge, A. H. Sakhaei, H. Lee, C. K. Dunn, N. X. Fang, M. L. Dunn, *Sci. Rep.* **2016**, *6*, 31110.

[188] J. Zotzmann, M. Behl, Y. Feng, A. Lendlein, *Adv. Funct. Mater.* **2010**, *20*, 3583.

[189] B. Peng, Y. Yang, K. Gu, E. J. Amis, K. A. Cavicchi, *ACS Mater. Lett.* **2019**, *1*, 410.

[190] N. Inverardi, S. Pandini, F. Bignotti, G. Scalet, S. Marconi, F. Auricchio, *Macromol. Mater. Eng.* **2020**, *305*, 1900370.

[191] X. Kuang, J. Wu, K. Chen, Z. Zhao, Z. Ding, F. Hu, D. Fang, H. J. Qi, *Sci. Adv.* **2019**, *5*, eaav5790.

[192] L. Hua, M. Xie, Y. Jian, B. Wu, C. Chen, C. Zhao, *ACS Appl. Mater. Interfaces* **2019**, *11*, 43641.

[193] H. Warren, M. in het Panhuis, G. M. Spinks, D. L. Officer, *J. Polym. Sci., Part B: Polym. Phys.* **2018**, *56*, 46.

[194] Y. Yang, Y. Tan, X. Wang, W. An, S. Xu, W. Liao, Y. Wang, *ACS Appl. Mater. Interfaces* **2018**, *10*, 7688.

[195] Y. Kim, H. Yuk, R. Zhao, S. A. Chester, X. Zhao, *Nature* **2018**, *558*, 274.

[196] J. Odent, S. Vanderstappen, A. Toncheva, E. Pichon, T. J. Wallin, K. Wang, R. F. Shepherd, P. Dubois, J.-M. Raquez, *J. Mater. Chem. A* **2019**, *7*, 15395.

[197] Z. Ji, C. Yan, B. Yu, X. Zhang, M. Cai, X. Jia, X. Wang, F. Zhou, *Adv. Mater. Technol.* **2019**, *4*, 1800713.

[198] C. H. Zhu, Y. Lu, J. Peng, J. F. Chen, S. H. Yu, *Adv. Funct. Mater.* **2012**, *22*, 4017.

[199] D. Han, Z. Lu, S. A. Chester, H. Lee, *Sci. Rep.* **2018**, *8*, 1963.

[200] M. Hippler, E. Blasco, J. Qu, M. Tanaka, C. Barner-Kowollik, M. Wegener, M. Bastmeyer, *Nat. Commun.* **2019**, *10*, 232.

[201] M. N. I. Shiblee, K. Ahmed, M. Kawakami, H. Furukawa, *Adv. Mater. Technol.* **2019**, *4*, 1900071.

[202] K. C. Hribar, R. B. Metter, J. L. Ifkovits, T. Troxler, J. A. Burdick, *Small* **2009**, *5*, 1830.

[203] H. Jiang, S. Kelch, A. Lendlein, *Adv. Mater.* **2006**, *18*, 1471.

[204] S. Lyu, F. Zheng, J. A. Aguilar-Tadeo, F. Lin, R. Wu, B. Derby, I. A. Kinloch, C. Soutis, M. Gresil, J. J. Blaker, *Soft Matter* **2020**, *16*, 1270.

[205] A. S. Gliozzi, M. Miniaci, A. Chiappone, A. Bergamini, B. Morin, E. Descrovi, *Nat. Commun.* **2020**, *11*, 2576.

[206] S. Xie, A. Natansohn, P. Rochon, *Chem. Mater.* **1993**, *5*, 403.

[207] H. S. Kang, S. Lee, J. K. Park, *Adv. Funct. Mater.* **2011**, *21*, 4412.

[208] V. Toshchevikov, M. Saphiannikova, G. Heinrich, *J. Phys. Chem. B* **2009**, *113*, 5032.

[209] P. Karageorgiev, D. Neher, B. Schulz, B. Stiller, U. Pietsch, M. Giersig, L. Brehmer, *Nat. Mater.* **2005**, *4*, 699.

[210] F. Pirani, A. Angelini, F. Frascella, R. Rizzo, S. Ricciardi, E. Descrovi, *Sci. Rep.* **2016**, *6*, 31702.

[211] I. Roppolo, A. Chiappone, A. Angelini, S. Stassi, F. Frascella, C. Pirri, C. Ricciardi, E. Descrovi, *Mater. Horiz.* **2017**, *4*, 396.

[212] J. L. Connell, E. T. Ritschdorff, J. B. Shear, *Anal. Chem.* **2016**, *88*, 12264.

[213] H. Lu, J. Leng, S. Du, *Soft Matter* **2013**, *9*, 3851.

[214] H. Luo, J. Hu, Y. Zhu, *Macromol. Chem. Phys.* **2011**, *212*, 1981.

[215] X. Peng, H. Wang, *J. Polym. Sci., Part B: Polym. Phys.* **2018**, *56*, 1314.

[216] Z. Zhao, X. Kuang, C. Yuan, H. J. Qi, D. Fang, *ACS Appl. Mater. Interfaces* **2018**, *10*, 19932.

[217] M. Jamal, A. M. Zarafshar, D. H. Gracias, *Nat. Commun.* **2011**, *2*, 527.

[218] a) S. Miao, H. Cui, M. Nowicki, L. Xia, X. Zhou, S. J. Lee, W. Zhu, K. Sarkar, Z. Zhang, L. G. Zhang, *Adv. Biosyst.* **2018**, *2*, 1800101; b) J. Wu, Z. Zhao, X. Kuang, C. M. Hamel, D. Fang, H. J. Qi, *Multifunct. Mater.* **2018**, *1*, 015002.

[219] Z. Zhao, J. Wu, X. Mu, H. Chen, H. J. Qi, D. Fang, *Macromol. Rapid Commun.* **2017**, *38*, 1600625.

[220] D. Jin, Q. Chen, T.-Y. Huang, J. Huang, L. Zhang, H. Duan, *Mater. Today* **2020**, *32*, 19.

[221] I. Must, F. Kaasik, I. Poldsalu, L. Mihkels, U. Johanson, A. Punning, A. Aabloo, *Adv. Eng. Mater.* **2015**, *17*, 84.

[222] W. Lehmann, H. Skupin, C. Tolksdorf, E. Gebhard, R. Zentel, P. Krüger, M. Lösche, F. Kremer, *Nature* **2001**, *410*, 447.

[223] G. M. Spinks, G. G. Wallace, L. S. Fifield, L. R. Dalton, A. Mazzoldi, D. De Rossi, I. I. Khayrullin, R. H. Baughman, *Adv. Mater.* **2002**, *14*, 1728.

[224] D. Han, C. Farino, C. Yang, T. Scott, D. Browe, W. Choi, J. W. Freeman, H. Lee, *ACS Appl. Mater. Interfaces* **2018**, *10*, 17512.

[225] D. Han, C. Yang, N. X. Fang, H. Lee, *Addit. Manuf.* **2019**, *27*, 606.

[226] Y.-W. Kang, J. Woo, H.-R. Lee, J.-Y. Sun, *Smart Mater. Struct.* **2019**, *28*, 095016.

[227] a) X. Yan, Q. Zhou, M. Vincent, Y. Deng, J. Yu, J. Xu, T. Xu, T. Tang, L. Bian, Y.-X. J. Wang, *Sci. Rob.* **2017**, *2*, eaaq1155; b) C. Peters,

**ADVANCED
SCIENCE NEWS**

www.advancedsciencenews.com

**ADVANCED
MATERIALS
TECHNOLOGIES**

www.advmattechnol.de

M. Hoop, S. Pané, B. J. Nelson, C. Hierold, *Adv. Mater.* **2016**, *28*, 533; c) U. Bozuyuk, O. Yasa, I. C. Yasa, H. Ceylan, S. Kizilel, M. Sitti, *ACS Nano* **2018**, *12*, 9617.

[228] W. Zhu, J. Li, Y. J. Leong, I. Rozen, X. Qu, R. Dong, Z. Wu, W. Gao, P. H. Chung, J. Wang, *Adv. Mater.* **2015**, *27*, 4411.

[229] X. Wang, X. H. Qin, C. Hu, A. Terzopoulou, X. Z. Chen, T. Y. Huang, K. Maniura-Weber, S. Pané, B. J. Nelson, *Adv. Funct. Mater.* **2018**, *28*, 1804107.

[230] X. Wang, X. Z. Chen, C. C. Alcântara, S. Sevim, M. Hoop, A. Terzopoulou, C. De Marco, C. Hu, A. J. de Mello, P. Falcaro, *Adv. Mater.* **2019**, *31*, 1901592.

[231] T. Xu, J. Zhang, M. Salehizadeh, O. Onaizah, E. Diller, *Sci. Rob.* **2019**, *4*, eaav4494.

[232] B. Wang, A. McDaid, M. Biglari-Abhari, T. Giffney, K. Aw, *Sens. Actuators, A* **2017**, *257*, 173.

[233] J. Shintake, V. Cacucciolo, D. Floreano, H. Shea, *Adv. Mater.* **2018**, *30*, 1707035.

[234] a) P. Rothemund, A. Ainla, L. Belding, D. J. Preston, S. Kurihara, Z. Suo, G. M. Whitesides, *Sci. Rob.* **2018**, *3*, eaar7986; b) R. V. Martinez, C. R. Fish, X. Chen, G. M. Whitesides, *Adv. Funct. Mater.* **2012**, *22*, 1376; c) K. P. Becker, Y. Chen, R. J. Wood, *Adv. Funct. Mater.* **2020**, *30*, 1908919; d) H. Yuk, S. Lin, C. Ma, M. Takaffoli, N. X. Fang, X. Zhao, *Nat. Commun.* **2017**, *8*, 14230.

[235] S. Y. Kim, R. Baines, J. Booth, N. Vasios, K. Bertoldi, R. Kramer-Bottiglio, *Nat. Commun.* **2019**, *10*, 3464.

[236] a) L. Ge, L. Dong, D. Wang, Q. Ge, G. Gu, *Sens. Actuators, A* **2018**, *273*, 285; b) X. Zheng, H. Lee, T. H. Weisgraber, M. Shusteff,

J. DeOtte, E. B. Duoss, J. D. Kuntz, M. M. Biener, Q. Ge, J. A. Jackson, *Science* **2014**, *344*, 1373.

[237] U. G. Wegst, H. Bai, E. Saiz, A. P. Tomsia, R. O. Ritchie, *Nat. Mater.* **2015**, *14*, 23.

[238] C. J. Thrasher, J. J. Schwartz, A. J. Boydston, *ACS Appl. Mater. Interfaces* **2017**, *9*, 39708.

[239] T. J. Wallin, L.-E. Simonsen, W. Pan, K. Wang, E. Giannelis, R. F. Shepherd, Y. Mengüç, *Nat. Commun.* **2020**, *11*, 4000.

[240] a) A. K. Mishra, T. J. Wallin, W. Pan, P. Xu, K. Wang, E. P. Giannelis, B. Mazzolai, R. F. Shepherd, *Sci. Rob.* **2020**, *5*, eaaz3918; b) M. De Volder, A. Moers, D. Reynaerts, *Sens. Actuators, A* **2011**, *166*, 111.

[241] H. Hsu, L.-Y. Liu, L.-Y. Liu, Y.-C. Su, *Smart Mater. Struct.* **2018**, *27*, 084006.

[242] M. Cavaiani, S. Dehaeck, Y. Vitry, P. Lambert, in *Int. Conf. on Manipulation Automation and Robotics at Small Scales*, MARSS, **2018**, https://doi.org/10.1109/MARSS.2018.8481145.

[243] T. Wallin, J. Pikul, S. Bodkhe, B. Peele, B. Mac Murray, D. Therriault, B. McEnerney, R. Dillon, E. Giannelis, R. Shepherd, *J. Mater. Chem. B* **2017**, *5*, 6249.

[244] X. Zheng, W. Smith, J. Jackson, B. Moran, H. Cui, D. Chen, J. Ye, N. Fang, N. Rodriguez, T. Weisgraber, *Nat. Mater.* **2016**, *15*, 1100.

[245] D. A. Walker, J. L. Hedrick, C. A. Mirkin, *Science* **2019**, *366*, 360.

[246] W. HuangáGoh, A. HoseináSakhaei, *J. Mater. Chem. B* **2018**, *6*, 3246.

Wenyu Zhao is an assistant engineer in the Shenzhen Institute of Artificial Intelligence and Robotics for Society. He received his bachelor's degree from the University of Science and Technology Beijing in materials science and engineering, and master's degree at Ecole Centrale de Lyon, France, in nanomaterials and engineering. His research focuses on the flexible pressure sensor, flow sensor, and 3D printing technologies.

Ziya Wang is currently an associate research fellow at Shenzhen Institute of Artificial Intelligence and Robotics for Society (AIRS). She received her Ph.D. in Physics from the University of Science and Technology Beijing in 2016. Her research interests are in smart materials, flexible electronics, and tactile perception in robots and soft robots.

**ADVANCED
SCIENCE NEWS**

www.advancedsciencenews.com

**ADVANCED
MATERIALS
TECHNOLOGIES**

www.advmattechnol.de

Jianpeng Zhang is currently a postdoctorate at Shenzhen University. He received his doctoral degree in solid mechanics from Beihang University in 2020. His research interests are in thermomechanical analysis and piezoresistive analysis of smart soft materials, mechanism of tactile perception of skin, and epidermal electronics.
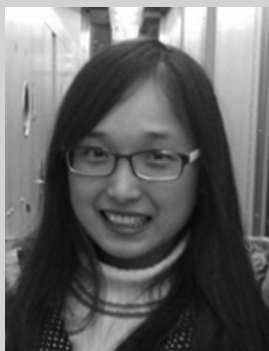
Xiaopu Wang received her doctoral degree in mechanical and processing engineering from ETH Zurich in 2020. Her work includes both fundamental study and application exploration of microrobots. Currently, she is an associate researcher at Shenzhen Institute of Artificial Intelligence and Robotics for Society (AIRS). She is also an adjunct assistant professor at the Chinese University of Hong Kong-Shenzhen (CUHK-SZ). Her research interests are in 3D printing, photopolymerization, untethered microrobots, and soft microactuators.

Yingtian Xu is an engineer of Shenzhen Institute of Artificial Intelligence and Robotics for Society. He received his bachelor's degree at Tianjin University in material forming and control engineering, and his M.S. degree in robotics from Johns Hopkins University. His research focuses on sensor-based robot control and voxel-based 3D topology structure generation.

Ning Ding received his Ph.D. from the Department of Mechanical and Automation Engineering, the Chinese University of Hong Kong, in 2013. He is currently the associate dean, Institute of Robotics and Intelligence Manufacturing, the Chinese University of Hong Kong, Shenzhen, and the director of the Center on Special Robots, Shenzhen Institute of Artificial Intelligence and Robotics for Society. His research interests are in computer vision, bioinspired robots.

**ADVANCED
SCIENCE NEWS**

www.advancedsciencenews.com

**ADVANCED
MATERIALS
TECHNOLOGIES**

www.advmattechnol.de

Zhengchun Peng received his Ph.D. in MEMS from the Georgia Institute of Technology, Atlanta, GA, in 2010. He then joined Intel Corp. as a senior R&D engineer. He is currently a distinguished professor at Shenzhen University. His main research interests are in the fields of flexible and stretchable electronics, nanosensors, MEMS, microfluidics, and tactile intelligence.